ORIGINAL PAPER

Reappraisal of early Paleogene CCD curves: foraminiferal assemblages and stable carbon isotopes across the carbonate facies of Perth Abyssal Plain

Haidi J. L. Hancock · Gerald R. Dickens · Ellen Thomas · Kevin L. Blake

Abstract Bulk carbonate content, planktic and benthic foraminiferal assemblages, stable isotope compositions of bulk carbonate and *Nuttallides truempyi* (benthic foraminifera), and non-carbonate mineralogy were examined across ~30 m of carbonate-rich Paleogene sediment at Deep Sea Drilling Project (DSDP) Site 259, on Perth Abyssal Plain off Western Australia. Carbonate content, mostly reflecting nannofossil abundance, ranges from 3 to 80% and generally exceeds 50% between 35 and 57 mbsf. A clay-rich horizon with a carbonate content of about 37% occurs between 55.17 and 55.37 mbsf. The carbonate-rich interval spans planktic foraminiferal zones P4c to P6b (~57–52 Ma), with the clay-rich horizon near the base of our Zone P5 (upper)—P6b. Throughout the studied interval, benthic species dominate foraminiferal assemblages, with scarce planktic foraminifera usually of poor preservation and limited species diversity. A prominent Benthic Foraminiferal Extinction Event (BFEE) occurs across the clay-rich horizon, with an influx of large *Acarinina* immediately above. The $\delta^{13}C$ records of bulk carbonate and *N. truempyi* exhibit trends similar to those observed in upper Paleocene–lower Eocene (~57–52 Ma) sediment from other locations. Two successive decreases in bulk carbonate and *N. truempyi* $\delta^{13}C$ of 0.5 and 1.0‰ characterize the interval at and immediately above the BFEE. Despite major changes in carbonate content, foraminiferal assemblages and carbon isotopes, the mineralogy of the non-carbonate fraction consistently comprises expanding clay, heulandite (zeolite), quartz, feldspar (sodic or calcic), minor mica, and pyrolusite (MnO_2). The uniformity of this mineral assemblage suggests that Site 259 received similar non-carbonate sediment before, during and after pelagic carbonate deposition. The carbonate plug at Site 259 probably represents a drop in the CCD from ~57 to 52–51 Ma, as also recognized at other locations.

Keywords Paleocene · Eocene · Carbonate · Planktic · Benthic · Carbon cycle

H. J. L. Hancock (✉)
Earth and Environmental Sciences, James Cook University, Townsville, QLD 4811, Australia
e-mail: Haidi.Hancock@jcu.edu.au

G. R. Dickens
Department of Earth Science, Rice University, Houston, TX 77005, USA

E. Thomas
Department of Geology and Geophysics, Yale University, P. O. Box 208109, New Haven, CT 06520-8109, USA

K. L. Blake
Advanced Analytical Centre, James Cook University, Townsville, QLD 4811, Australia

Introduction

Deep ocean temperatures and dissolved inorganic carbon concentrations underwent profound changes during the early Paleogene (~60–50 Ma) as evidenced by a characteristic series of shifts in the oxygen and carbon isotope compositions ($\delta^{18}O$ and $\delta^{13}C$) of benthic foraminiferal carbonate (e.g., Zachos et al. 2001) (Fig. 1). The most prominent $\delta^{13}C$ high of the Cenozoic occurred during the late Paleocene (~59–56 Ma), a time of transition from relatively cool to relatively warm bottom water temperatures. Presumably, this
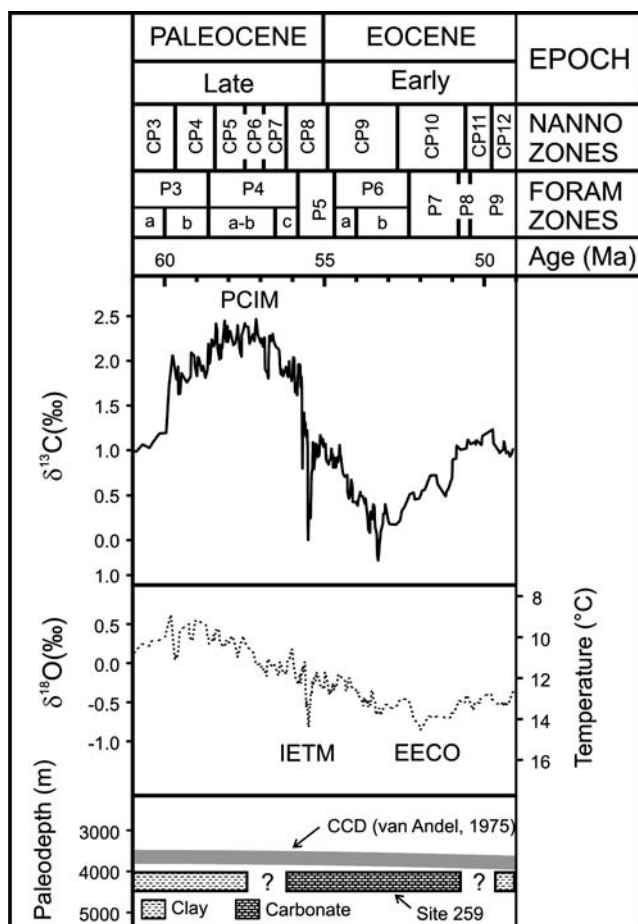
Fig. 1 Global carbon and oxygen isotope curves constructed from benthic foraminiferal isotope data (adapted from Zachos et al. 2001, p 688). Also shown are (*grey band*) the reconstructed early Palaeogene calcite compensation depth (*CCD*) for the Indian Ocean (adapted from van Andel 1975), and (*bricks*) the approximate depth and age of the carbonate unit at DSDP Site 259. *PCIM* Paleocene carbon isotope maximum, *IETM* initial Eocene thermal maximum, *EECO* Early Eocene climatic optimum

Paleocene Carbon Isotope Maximum (PCIM) reflects massive deposition of organic carbon (Shackleton and Hall 1984), although the location of the output remains uncertain (Corfield 1994; Kurtz et al. 2003; Hollis et al. 2005). The PCIM was followed by continued rise in deep ocean temperatures and a decline in benthic foraminiferal δ^{13}C. At least one brief event marked by extreme warming and depletion in δ^{13}C punctuated these trends at the Paleocene/Eocene (P/E) boundary ~55.5 Ma (e.g., Kennett and Stott 1991). The negative carbon isotope excursion (CIE) during this <200 kyear event, referred to here as the Initial Eocene Thermal Maximum (IETM), signifies a massive injection of ^{13}C-depleted carbon to the ocean and atmosphere (Dickens et al. 1997; Katz et al. 1999). After the CIE and a partial recovery to pre-event conditions, benthic fora-

miniferal δ^{13}C records plunged to a low centered at ~53 Ma. This interval of anomalous δ^{13}C values may include one or more IETM-like events or hyperthermals, each associated with a δ^{13}C minimum (Thomas and Zachos 2000; Thomas et al. 2000; Cramer et al. 2003; Lourens et al. 2005); it also ushers in the early Eocene Climatic Optimum (EECO), the time of peak Cenozoic global temperatures.

Carbonate accumulation in marine sediment removes a large fraction of carbon from the ocean–atmosphere system (Kump and Arthur 1999; Katz et al. 2005). However, this output is spatially heterogeneous because extensive regions of the seafloor lie beneath the calcite compensation depth (CCD), a horizon marking the lower limit of carbonate occurrence in marine sediment and reflecting the saturation state of calcite in deep seawater (Murray and Renard 1891; Peterson 1966). Physiochemical conditions of the deep ocean and in near-seafloor sediments, especially pressure, temperature and the activities of Ca^{2+} and CO_3^{2-}, regulate the CCD (Valyashko et al. 1989; Pearson and Palmer 2000; Tyrrell and Zeebe 2003). One consequence of these controls is that the modern CCD generally varies in mid-latitude regions from ~4,400 m below sea level (mbsl) in the cold, CO_2–rich bottom waters of the Pacific to 5,200 mbsl in the relatively warm, CO_2–deficient bottom waters of the Atlantic (Berger and von Rad 1972; van Andel 1975; Berger et al. 1976). Another effect is that the ratio of carbonate to organic carbon reaching the seafloor impacts calcite preservation so that the CCD is depressed beneath areas of high surface water carbonate production, such as the equator (Archer and Maier-Reimer 1994; Mekik et al. 2002).

In a now classic paper, van Andel (1975) extended earlier work (Berger and von Rad 1972) to reconstruct the position of the CCD in the Atlantic, Indian and Pacific Oceans from the Late Jurassic to present-day. These curves, which have remained the standard for models of Cenozoic global geochemical cycling (e.g., Tyrrell and Zeebe 2003), show the CCD fluctuating by more than 1,200 m over the last 50 myear. Given the aforementioned major changes in deep ocean temperature and carbon cycling during the early Paleogene, one might predict significant fluctuations in the CCD to have occurred between 60 and 50 Ma, but compilations (Berger and von Rad 1972; van Andel 1975) show a fairly shallow (~3.5 km) and relatively unchanging (<200 m) CCD in all oceans during this time (Fig. 1).

The long-term CCD curves generated by van Andel (1975) used sections recovered by scientific drilling prior to 1975. The paleodepths of Deep Sea Drilling Project (DSDP) sites were backtracked over time, and

dated intervals of carbonate and clay were projected onto these trajectories. However, some intervals of lower Paleogene carbonate preservation or dissolution were either not recognized or specifically excluded. One example is the ~3 m thick carbonate-poor unit at ~150 m below seafloor (mbsf) at DSDP Site 213 in the northeastern Indian Ocean. This horizon, perhaps overlooked in 1975 because it lies atop basement, marks the IETM (Ravizza et al. 2001) and a rapid shoaling of the CCD in intermediate waters (Dickens et al. 1997). Of particular interest to this investigation is a 31 m thick unit of lower Paleogene carbonate sandwiched between clays at DSDP Site 259 in the eastern Indian Ocean. Preliminary interpretations suggested that this sedimentary unit reflected a drop in the CCD (Shipboard Scientific Party 1974), but it was omitted in the compilations by van Andel (1975) because, at the time, "a temporary deepening of the CCD (during the early Paleogene seemed) unreasonable in the light of other evidence".

Two recent studies highlight a potential problem with the early Paleogene portion of the van Andel (1975) CCD curves. Zachos et al. (2004) presented Cenozoic records of carbonate accumulation on Walvis Ridge in the southeastern Atlantic Ocean, and Hancock and Dickens (2005) published Paleogene records of carbonate dissolution on Shatsky Rise in the northern Pacific. Both show an interval of high carbonate accumulation and preservation between ~57 and 51 Ma, suggesting a significant drop in the CCD and prompting us to re-examine the calcareous unit at DSDP Site 259. Most lower Paleogene sections recovered by DSDP and ODP accumulated at water depths too shallow or too deep to monitor fluctuations in the CCD. Site 259 is one of few locations drilled to date with sediment core deposited between 4,000 and 4,500 m water depth during the early Paleogene. However, with available information, it is difficult to place the observed record at this site into a paleoceanographic context. We establish the nature and timing of this carbonate "plug", and argue that it indeed represents a deepening of the CCD from the late Paleocene through the early Eocene (~57–52 Ma), comparable with records from Walvis Ridge and Shatsky Rise.

## Site 259 and lower Paleogene abyssal carbonate

DSDP Site 259 is located on Perth Abyssal Plain in the southern Indian Ocean off the western Australian margin (Fig. 2). At present, the site lies at 29°37.05′S, 112°41.78′E, and 4,696 mbsl. During the early Paleo-
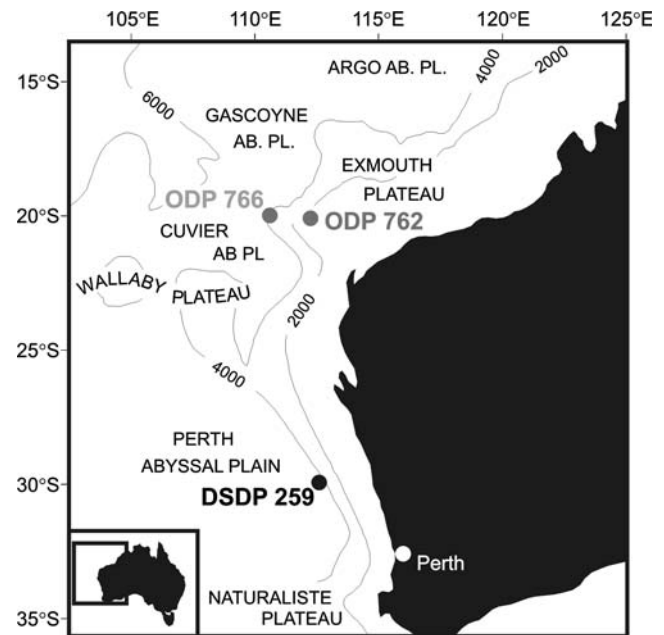
Fig. 2 Present location of DSDP Site 259 in the Perth Abyssal Plain offshore Western Australia. Also shown are the locations of ODP Sites 762 and 766, which are discussed in the text

gene, however, Site 259 was much farther south, at approximately 55°S (Ocean Drilling Stratigraphic Network http://www.odsn.de).

Drilling at Site 259 penetrated through 304 m of pelagic sediment and 42 m of basalt (Shipboard Scientific Party 1974). The basalt is tholeiitic, similar to that found at modern mid-ocean ridges (Robinson and Whitford 1974; Thompson et al. 1978). It presumably formed at a spreading ridge in the Early Cretaceous, based on the regional tectonic history and the conformable contact with overlying Aptian sediment (Thompson et al. 1978; Veevers and Tayton 1985). Assuming a typical water depth for the center of this ridge (2,500 m) and normal subsidence rates, the site likely lay beneath 4,000 m of water during the Late Cretaceous and early Paleogene (van Andel 1975). The upper Albian–middle Paleogene sedimentary succession comprises zeolitic clay, indicating a depth below the CCD (Shipboard Scientific Party 1974), but yellowish-orange lower Paleogene nannofossil clay and ooze was recovered between 60 and 29 mbsf (Fig. 3). Lower Paleogene nannofossil ooze also outcrops on the seafloor 10 km south of Site 259, where the water is about 100 m deeper (Shipboard Scientific Party 1974). This suggests a laterally extensive deposit of lower Paleogene pelagic or hemipelagic carbonate. At Site 259, the calcareous unit is overlain by 26 m of zeolitic clay (age unknown) and Quaternary foraminifera-bearing nannofossil ooze (uppermost core).
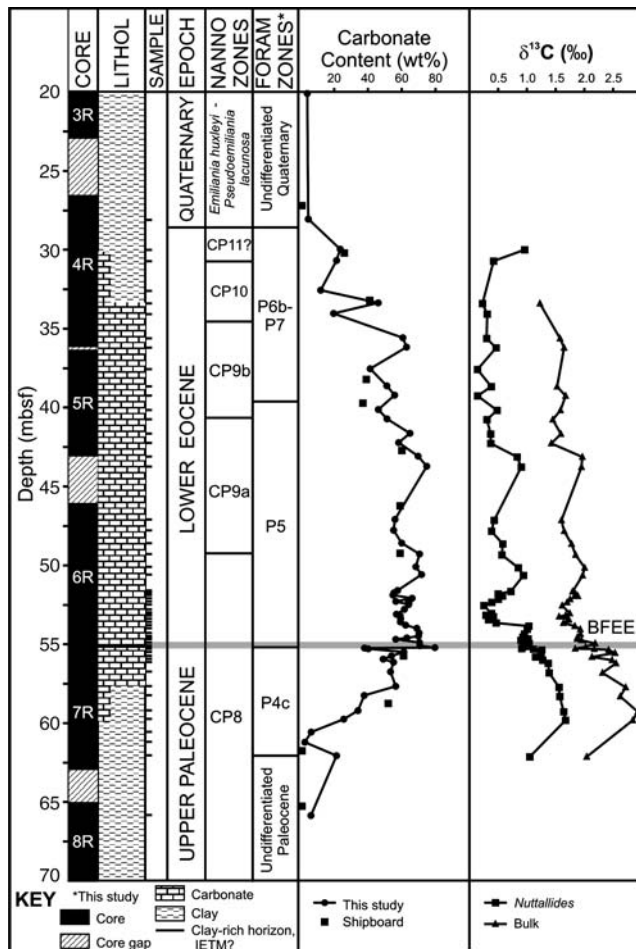
Fig. 3 The stratigraphic record at DSDP Site 259 between 20 and 70 m below seafloor showing core placement, lithology, sample location, shipboard biostratigraphy (Proto-Decima 1974), bulk carbonate content, and the carbon isotope composition of bulk sediment and the benthic foraminifera *Nuttallides truempyi*

Initial biostratigraphic work (Krasheninnikov 1974; Proto-Decima 1974) indicated that the calcareous unit is dominated by solution-resistant nannofossil and foraminiferal tests deposited from the late Paleocene through early Eocene. Five nannofossil zones were identified, although drilling disturbance or sediment re-deposition apparently caused some repetition of zones (Proto-Decima 1974, Table 3, p 593). These are the *Discoaster multiradiatus, Tribrachiatus contortus, Discoaster binodosus, Tribrachiatus orthostylus*, and *Discoaster lodoensis* zones, corresponding to zones CP8 through CP11 following Berggren et al. (1995) (Fig. 3). Planktic and benthic foraminifera were also examined (Krasheninnikov 1974), but without information on sample depths, a range chart, or photographic documentation of taxa. The main findings of this work were: (1) planktic foraminifera are rare but benthic foraminifera are relatively common; (2) planktic foraminif-

eral assemblages comprised the *Globorotalia velascoensis* (=*Morozovella velascoensis*), *Gl. subbotinae* (=*M. subbotinae*), and *Gl. formosa formosa* (=*M. formosa*) zones; and (3) foraminiferal assemblages are probably affected by dissolution. The P/E Boundary, either as originally defined or currently correlated to the start of the IETM (Aubry et al. 2003; Dupuis et al. 2003), was not located (Krasheninnikov 1974). To our knowledge, no stable isotope records have been generated across the calcareous unit at Site 259.

Samples and methods

Sixty samples of ~20 cm³ were collected from 20 to 62 mbsf, a depth interval which spans the calcareous unit (Fig. 3). Samples were initially collected every 1 m, but after examination of foraminiferal assemblages and carbon isotope values (discussed below) sampling frequency was increased to every 20 cm across the IETM.

All samples were freeze-dried to remove pore water, lightly homogenized, and divided into two portions. An ~5 cm³ portion was crushed to determine bulk carbonate content and stable isotope composition. A ~10 cm³ portion was wet sieved at 63 μm and dried to examine sediment characteristics and foraminifera.

Carbonate contents were analyzed using the ''Karbonate-Bombe'' method (Mueller and Gastner 1971). All samples were analyzed twice to increase precision. A sample of Paleogene siliceous limestone with a known CaCO₃ content of 72 wt% was analyzed three times to evaluate accuracy and precision. These analyses rendered a CaCO₃ content of 72 ± 1.5 wt%.

The second portion was passed through a microsplitter and separated into two aliquots for optical microscopic examination. One aliquot was analyzed for sediment characteristics and planktic foraminifera, the other for benthic foraminifera. Planktic foraminifera are rare (Krasheninnikov 1974), but many specimens were examined using a Jeol JSM 5410LV scanning electron microscope (SEM) at the James Cook University Advanced Analytical Centre (JCU-AAC).

Planktic foraminiferal species were identified and named in accordance with established Paleocene (Olsson et al. 1999) and Eocene classifications (Toumarkine and Luterbacher 1985). Eocene species were discussed with Bill Berggren and Dick Olsson in personal communications. To establish sediment age, planktic foraminiferal assemblages were placed into the zonal scheme presented by Berggren et al. (1995), with modifications made by Olsson et al. (1999) and Hancock et al. (2002). The latter work details early

Paleogene planktic foraminiferal assemblages at ODP Site 762 on Exmouth Plateau, a location fairly close to Site 259 (Fig. 2).

Benthic foraminifera were picked from the >63 μm size fraction and determined to the species level for common or paleoenvironmentally significant taxa. Generic assignment was made for other taxa. For instance, no species were determined within the group of *Laevidentalina* spp. and unilocular genera. Taxonomy at the generic level follows Loeblich and Tappan (1988); that at the specific level follows Tjalsma and Lohmann (1983), van Morkhoven et al. (1986), Thomas (1990), Nomura (1991), Bolli et al. (1994), Widmark (1997), and Alegret and Thomas (2001). Data are given in a presence/absence format. We did not analyze the benthic faunas quantitatively because in many samples a large number of specimens were not well preserved. We identified between 150 and 300 specimens per sample. We followed van Morkhoven et al. (1986) in paleobathymetric assignments.

Samples of bulk carbonate and *Nuttallides truempyi* specimens were analysed for their stable isotope compositions. *Nuttallides truempyi* is a common, cosmopolitan Late Cretaceous-Eocene, bathyal-abyssal species, which is often used for isotope work, including recently published global compilations (Zachos et al. 2001; Katz et al. 2003). Although *Nuttallides truempyi* specimens show little variation in $\delta^{13}C$ across size fractions, only average-sized specimens (125–250 μm diameter) were used. Thirty to 40 specimens from each sample were analyzed. One set of samples was analyzed at the Earth Sciences Centre, Gothenburg, Sweden, with a VG Prism Series II mass spectrometer attached to an Isocarb preparation system. Another set of samples was analyzed at the Department of Geological Sciences, University of California, Santa Barbara, with a Finnigan MAT 251 mass spectrometer connected to a carousel-48 automated carbonate preparation device, which has a common reaction vessel (orthophosphoric acid). Analytical precision was less than 0.1‰ for both sets of analyses. Replicates of two samples analysed at both laboratories were within 0.15‰. Oxygen isotopes were determined for all samples, but are not discussed in this paper.

The mineralogy of the non-carbonate fraction was examined for six samples from below, within and above the carbonate unit. Dried and crushed samples were reacted with 10% HCl to remove $CaCO_3$. Resulting slurries were rinsed with H_2O several times, and dried in an oven at 40°C for 2 days. The residues were prepared as powder mounts, for which approximately 0.5 g of sample was re-crushed and packed into a plastic cavity. Analyses were conducted using a Siemens D5000 X-ray Diffractometer housed at the JCU-AAC. This instrument is fitted with a copper tube (Cu Kα = 1.54178 Å), operating at 40 kV and 30 mA, and a post-diffraction graphite monochromator. Sample residues were scanned from 1.3° to 65° 2θ in steps of 0.02° 2θ at 2.4 s per step.

Results

Carbonate contents

Carbonate content over the studied interval varies from 3 to 80% (Table 1; Fig. 3). In general, carbonate content increases down-hole from 29 mbsf to a broad high between 35 and 57 mbsf, where values usually exceed 50%. The carbonate content declines down-hole, dropping to less than 7% by 60 mbsf. Overall, the values and trend agree with previous measurements (Bode 1974), and the shipboard descriptions of "light brown nannofossil clay and ooze" (Shipboard Scientific Party 1974). No sample analyzed between 35 and 57 mbsf has a carbonate content less than 37%, concurring with shipboard descriptions, which do not indicate clay horizons within this depth interval.

Planktic foraminiferal biostratigraphy

Planktic foraminifera are absent in samples from outside the calcareous unit (>62.01 and <20.10 mbsf). Within the carbonate plug, planktic foraminifera are usually poorly preserved and show heavy secondary calcite overgrowths (Fig. 4). They consistently comprise <5% of the >63 μm size fraction and many samples do not contain identifiable planktic specimens. The ratio of benthic foraminifera to planktic foraminifera usually exceeds 20:1. In the impoverished planktic foraminiferal assemblages, the thick-walled *Acarinina* and *Subbotina* generally dominate samples below 50 mbsf, whereas *Chiloguembelina wilcoxensis* dominates samples above 50 mbsf, in general agreement with Krasheninnikov (1974).

Some samples contain stratigraphically important species (Fig. 4). On the basis of first appearance datums (FADs) or last appearance datums (LADs) of these species, the calcareous unit approximately ranges from subzones P4c to P6b of the sub-tropical global scheme, or ~57 to ~52 Ma (Berggren et al. 1995) (Table 2; Fig. 3). The planktic foraminiferal assemblages

Table 1 Hancock et al. Paleogene CCD	Sample: leg, hole, core, section, interval (cm)	Depth (mbsf)	Carbonate content (wt%) (this study)	Depth (mbsf)	Carbonate content (wt%) (ship)
	27-259-3R-2, 110–116	20.10	4.19	27.2	1
	27-259-4R-1, 60–65	28.06	4.78	30.2	26
	27-259-4R-2, 100–105	29.96	23.62	33.2	41
	27-259-4R-3, 22–26	30.68	21.43	38.2	39
	27-259-4R-4, 60–65	32.56	12.03	39.7	37
	27-259-4R-4, 140–144	33.36	46.10	42.7	60
	27-259-4R-5, 57–62	34.03	19.66	46.2	59
	27-259-4R-6, 61–66	35.57	60.66	49.2	59
	27-259-4R-6, 120–124	36.16	62.84	52.2	64
	27-259-5R-1, 103–108	37.53	41.30	55.7	61
	27-259-5R-2, 61–66	38.61	51.18	58.7	52
	27-259-5R-2, 120–124	39.2	55.77	61.7	1
	27-259-5R-3, 61–66	40.11	46.12	65.2	1
	27-259-5R-3, 120–124	40.7	51.28		
	27-259-5R-4, 61–66	41.61	64.83		
	27-259-5R-4, 120–124	42.2	58.17		
	27-259-5R-5, 56–61	43.06	69.64		
	27-259-5R-5, 120–124	43.7	74.76		
	27-259-6R-1, 51–56	47.06	56.01		
	27-259-6R-1, 120–124	47.75	55.17		
	27-259-6R-2, 51–56	48.56	59.95		
	27-259-6R-2, 120–124	49.25	70.52		
	27-259-6R-3, 51–56	50.06	68.31		
	27-259-6R-3, 100–104	50.55	71.70		
	27-259-6R-4, 51–56	51.56	57.54		
	27-259-6R-4, 66–70	51.71	55.36		
	27-259-6R-4, 80–84	51.85	54.82		
	27-259-6R-4, 100–104	52.05	66.11		
	27-259-6R-4, 120–124	52.25	56.49		
	27-259-6R-4, 140–144	52.45	64.07		
	27-259-6R-5, 20–24	52.75	61.55		
	27-259-6R-5, 51–56	53.06	56.86		
	27-259-6R-5, 60–64	53.15	59.07		
	27-259-6R-5, 80–84	53.35	59.34		
	27-259-6R-5, 100–104	53.55	59.21		
	27-259-6R-5, 120–124	53.75	62.28		
	27-259-6R-5, 140–144	53.95	68.92		
	27-259-6R-6, 20–24	54.25	70.27		
	27-259-6R-6, 40–44	54.45	69.88		
	27-259-6R-6, 51–56	54.56	62.99		
	27-259-6R-6, 60–64	54.65	56.44		
	27-259-6R-6, 80–84	54.85	70.46		
	27-259-6R-6, 100–104	55.05	70.72		
	27-259-6R-6, 112–115	*55.17*	*79.61*		
	27-259-6R-6, 115–118	*55.2*	*37.94*		
	27-259-6R-6, 120–124	*55.25*	*40.23*		
	27-259-6R-6, 140–144	55.45	61.25		
	27-259-7R-1, 20–24	55.70	53.92		
	27-259-7R-1, 40–44	55.90	49.02		
	27-259-7R-1, 60–65	56.10	55.14		
	27-259-7R-1, 120–124	56.7	53.35		
	27-259-7R-2, 62–65	57.62	56.42		
	27-259-7R-2, 120–124	58.2	37.82		
	27-259-7R-3, 66–69	59.16	34.11		
	27-259-7R-3, 120–124	59.7	25.68		
Carbonate content (wt%) this study and Shipboard Scientific Party (1974). IETM interval is in italics	27-259-7R-4, 52–57	60.52	6.46		
	27-259-7R-4, 116–120	61.16	2.70		
	27-259-7R-5, 51–56	62.01	21.44		
	27-259-8R-1, 80–85	65.80	6.29		
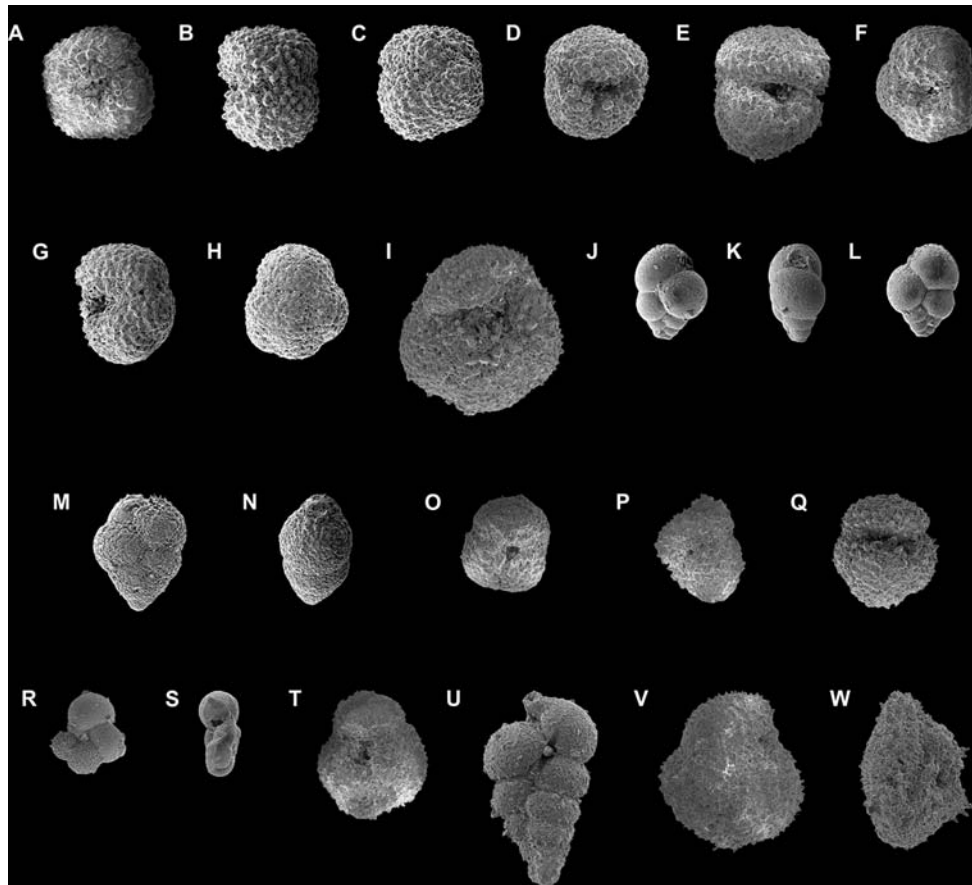
Fig. 4 Magnification: 1 cm = 100 μm. Scanning Electron Microscope (*SEM*) photographs of Paleocene and Eocene planktic foraminifera, Site 259. **a–e** *Acarinina coalingensis* (Cushman and Hanna 1927): **a** ventral view, **b** side view, **c** spiral view, **d** side view, **e** ventral view (259-6R-5, 40–44 cm). **f, g, h** *Acarinina nitida* (Martin 1943): **f** ventral view, **g** side view, **h** spiral view (259-7R-5, 51–56 cm). **i** *Acarinina soldadoensi* (Bronnimann 1952): ventral view. **j, k, l** *Chiloguembelina crinita* (Glaessner 1937): **j** ventral view, **k** side view, **l** spiral view (259-6R-5, 51–56 cm). **m, n** *Chiloguembelina wilcoxensis* (Cushman and Ponton 1932): **m** ventral view, **n** side view (259-6R-3, 51–56 cm). **o** ?*Glob-* *igerinatheka senni* (Beckmann 1953): ventral view (259-5R-2, 120–124 cm). **p** *Morozovella lensiformis* (Subbotina 1953): side view (259-5R-2, 120–124 cm). **q** *Acarinina primitiva* (Finlay 1947): ventral view (259-6R-5, 40–44 cm). **r, s** *Species 1* (to be described in forthcoming Eocene atlas, Pearson et al.); **r** ventral view (259-5R-2, 120–124 cm), **s** side view (259-4R-4, 140–144 cm). **t.** *Acarinina wilcoxensis* (Cushman & Ponton, 1932): ventral view (259-6R-6, 112–116 cm). **u** *Zeauvigerina zealandica* (Finlay 1939) (259-5R-2, 120–124 cm). **v, w** *Morozovella subbotinae* (Morozova 1939): **v** ventral view, **w** side view (259-5R-2, 120–124 cm)

are too poorly preserved to assess whether cores within this interval contain duplicate sediment horizons, as suggested by previous nannofossil work (Proto-Decima 1974).

Subzone P4c (62.01–55.17 mbsf)

The FADs of the primary marker species, *Acarinina soldadoensis*, and secondary marker species, *A. coalingensis*, for Subzone P4c occur at 55.7 mbsf. However, these species could have appeared earlier given the extremely poor preservation of planktic foraminifera below 55.7 mbsf. *Chiloguembelina wilcoxensis* and *Acarinina nitida* both first occur at 62.01 mbsf. The co-occurrence of these species identifies lowermost Subzone P4c at other locations (Olsson et al. 1999). The domination of Subzone P4c assemblages by *Acarinina* and *Subbotina* is typical for mid-high latitude locations (e.g., Stott and Kennett 1990; Quillevere and Norris 2003).

Krasheninnikov (1974) assigned Cores 8, 7 and 6 (and tentatively the bottom of core 5) to the upper Paleocene *Acarinina acarinata* (=*A. nitida*) Zone, noting, that *A. acarinata* was the most common species below 40 mbsf. Other species identified by this author included *Acarinina mckannai*, *A. primitiva*, *A.* sp., *Globigerina chascanona*, *G. nana*, *Chiloguemblina* aff. *wilcoxensis*, and rare *Globorotalia* aff. *acuta*. These species are representative of Subzone P4c (Berggren et al. 1995). A P4c planktic foraminiferal zonal

Table 2 Hancock et al. Paleogene CCD

Sample	Depth (mbsf)	Foram Zone (Berggren et al., 1995)	Acarinina nitida	Subbotina velascoensis	Chiloguembelina wilcoxensis	Chiloguembelina crinita	Subbotina spp	Acarinina mckannai	Acarinina soldadoensis	Acarinina coalingensis	Globanomalina spp.	Acarinina primitiva	Acarinina wilcoxensis	?Acarinina subsphaerica	Zeauvigerina zealandica	Morozovella subbotinae	?Globigerinatheka senni	Morozovella lensiformis	Species I.
27-259-3R-2, 110-116	20.10	?																	
27-259-4R-1, 60-65	28.06	P6b																	
27-259-4R-2, 100-105	29.96																		
27-259-4R-3, 22-26	30.68						X												
27-259-4R-4, 60-65	32.5					X			X										
27-259-4R-4, 140-144	33.36																		X
27-259-4R-5, 57-62	34.03			X			X												
27-259-4R-6, 61-66	35.57			X															
27-259-4R-6, 120-124	36.16			X					X	X			X		X				
27-259-5R-1, 103-108	37.53			X	X		X		X	X									
27-259-5R-2, 61-66	38.61X						X												
27-259-5R-2, 120-124	39.20			X	X		X					X			X		X	X	X
27-259-5R-3, 61-66	40.11	P5 (upper) - P6a		X					X										
27-259-5R-3, 120-124	40.70																		
27-259-5R-4, 61-66	41.61			X															
27-259-5R-4, 120-124	42.20			X			X								X				
27-259-5R-5, 56-61	43.06																		
27-259-5R-5, 120-124	43.70			X			X		X	X		X		X	X	X			
27-259-6R-1, 51-56	47.06			X															
27-259-6R-1, 120-124	47.75			X					X										
27-259-6R-2, 51-56	48.56						X												
27-259-6R-2, 120-124	49.25			X	X		X		X	X		X							
27-259-6R-3, 51-56	50.06		X	X						X									
27-259-6R-3, 100-104	50.55																		
27-259-6R-4, 51-56	51.56				X														
27-259-6R-4, 66-70	51.71																		
27-259-6R-4, 80-84	51.85																		
27-259-6R-4, 100-104	52.05																		
27-259-6R-4, 120-124	52.25																		
27-259-6R-4, 140-144	52.45																		
27-259-6R-5, 20-24	52.75																		
27-259-6R-5, 51-56	53.06			X	X														
27-259-6R-5, 60-64	53.15			X															
27-259-6R-5, 80-84	53.35			X															
27-259-6R-5, 100-104	53.55																		
27-259-6R-5, 120-124	53.75			X		X			X			X	X						
27-259-6R-5, 140-144	53.95																		
27-259-6R-6, 20-24	54.25																		
27-259-6R-6, 40-44	54.45																		
27-259-6R-6, 51-56	54.56			X	X		X			X									
27-259-6R-6, 60-64	54.65																		
27-259-6R-6, 80-84	54.85																		
27-259-6R-6, 100-104	55.05																		
27-259-6R-6, 112-115	55.17		X						X	X	X	X	X						
27-259-6R-6, 115-118	55.20	P4c																	
27-259-6R-6, 120-124	55.25																		
27-259-6R-6, 140-144	55.45																		
27-259-7R-1, 20-24	55.70		X					X	X	X									
27-259-7R-1, 40-44	55.90																		
27-259-7R-1, 60-65	56.10																		
27-259-7R-1, 120-124	56.70					X													
27-259-7R-2, 62-65	57.62																		
27-259-7R-2, 120-124	58.20																		
27-259-7R-3, 66-69	59.16																		
27-259-7R-3, 120-124	59.70																		
27-259-7R-4, 52-57	60.52																		
27-259-7R-4, 116-120	61.16																		
27-259-7R-5, 51-56	62.01		X	X	X	X													
27-259-8R-1, 80-85	65.80	?																	

Planktic foraminiferal biostratigraphy, Site 259. Gray shaded area is the IETM interval and black line denotes BFEE

assignment for this depth interval is consistent with the CP8 nannofossil Zone suggested by Proto-Decima (1974).

Zone P5 (upper): subzone P6a (55.17–39.2 mbsf)

The primary marker species for the base of Zone P5, *Globanomalina psuedomenardii*, is absent at Site 259. However, the FAD of *Acarinina wilcoxensis* is recognized at 55.17 mbsf, and this datum occurs within upper Zone P5 in the tropical–subtropical scheme (Berggren et al. 1995). Large and robust variants of *A. coalingensis* dominate the foraminiferal assemblages at 55.17 mbsf. An abrupt increase in large and robust variants of *A. coalingensis* and *A. soldadoensis* has been reported at other high southern latitude sites during the IETM (Kelly 2002). The FAD of *A. primitiva*, which is the more quadrate chambered end member of the *A. coalingensis–A. primitiva* lineage, also occurs at 55.17 mbsf. Although this datum approximates the base of Zone P7 in some locations (Huber 1991; Kelly 2002), it marks the P/E boundary at other high southern latitude sites (Hancock et al. 2003; Hollis et al. 2005). *Morozovella subbotinae* was identified in one sample at 43.70 mbsf, and this species is a very common constituent of Zone P5 through Subzone P6a assemblages elsewhere (Olsson et al. 1999).

The LAD of *Morozovella velascoensis* marks the base of Subzone P6a (Berggren et al. 1995). However, this species was not found at Site 259 so that Zone P5 and Subzone P6a, cannot be discriminated. *Morozovella velascoensis* is absent or extremely rare at other high to middle latitude sites of the southern hemisphere (e.g., Hancock et al. 2002; Zachos et al. 2004).

Krasheninnikov (1974) failed to identify the P/E boundary, and assigned most of this depth interval to the upper Paleocene *Acarinina acarinata* Zone. On the basis of nannofossils, the P/E boundary was placed at 36.5 mbsf (Shipboard Scientific Party 1974) and 41.4 mbsf (Proto-Decima 1974). Such placements are inconsistent with the planktic foraminiferal assemblages described in this study (and other information, below), which indicate that the P/E boundary occurs at ~55.17 mbsf. We note, though, that definition of the P/E boundary in deep-sea sediments was a contentious issue until the boundary was finally correlated to the base of the CIE (Dupuis et al. 2003).

Subzone P6b (39.2–27 mbsf)

The FAD of *Morozovella lensiformis* marks the base of this subzone and occurs at 39.2 mbsf. Planktic forami-

niferal assemblages are characterized by *Acarinina primitiva*, *A. soldadoensis*, *Chiloguembelina wilcoxensis*, *Ch. trinitatensis* and *Zeauvigerina zealandica*, and these species are typically found in P6b assemblages elsewhere (Berggren and Olsson, personal communication, 2004/2005).

Although we identified very few planktic foraminifera in samples from above Core 5 (i.e., 36.5 msf, Table 2), Krasheninnikov (1974) found casts of *Morozovella aequa*, *M. subbotinae* and *M. marginodentata* in Sect. 3 of Core 4. This core was thus assigned to the *Globorotalia subbotinae* (=*Morozovella subbotinae*) and the *Gl. formosa formosa* (=*M. formosa*) zones (lower part of lower Eocene). These observations are in good agreement with the CP9b nannofossil zonal assignment by Proto-Decima (1974).

Undifferentiated

Samples from sediment intervals below and above the calcareous unit are assigned to undifferentiated upper Paleocene and undifferentiated upper Quaternary, respectively, on the basis of nannofossil assemblages (Proto-Decima 1974).

Benthic foraminifera

The composite faunal list for benthic foraminifera comprises 82 mostly calcareous taxa (Table 3), some of which are illustrated in this paper (Fig. 5). Preservation is generally moderate, but varies strongly between samples. The Paleocene assemblages are dominated by large epifaunal species, generally interpreted as reflecting relatively oligotrophic and well-oxygenated environments (e.g., Alegret and Thomas 2001). The overall assemblage is consistent with an abyssal depositional environment (Thomas 1998), and the high diversity is common for early Paleogene sediments (e.g., Nomura 1991; Thomas and Zachos 1999). Preservation is generally moderate, but varies strongly between samples. The size of benthic foraminiferal specimens varies significantly within each sample, so that common species such as *Nuttallides truempyi* are represented by medium (125–250 μm) to very large (>250–300 μm) tests. All samples sieved for benthic foraminifera also contain large (>250 μm) and commonly rounded quartz grains.

Benthic foraminiferal species generally restricted to the Paleocene have been reworked from shallow samples. However, these specimens can generally be recognized by poor preservation, and a benthic foraminiferal extinction is recognized between samples 27-259-6R-6, 115–118 (55.20 mbsf) and 27-259-6R-6, 112–
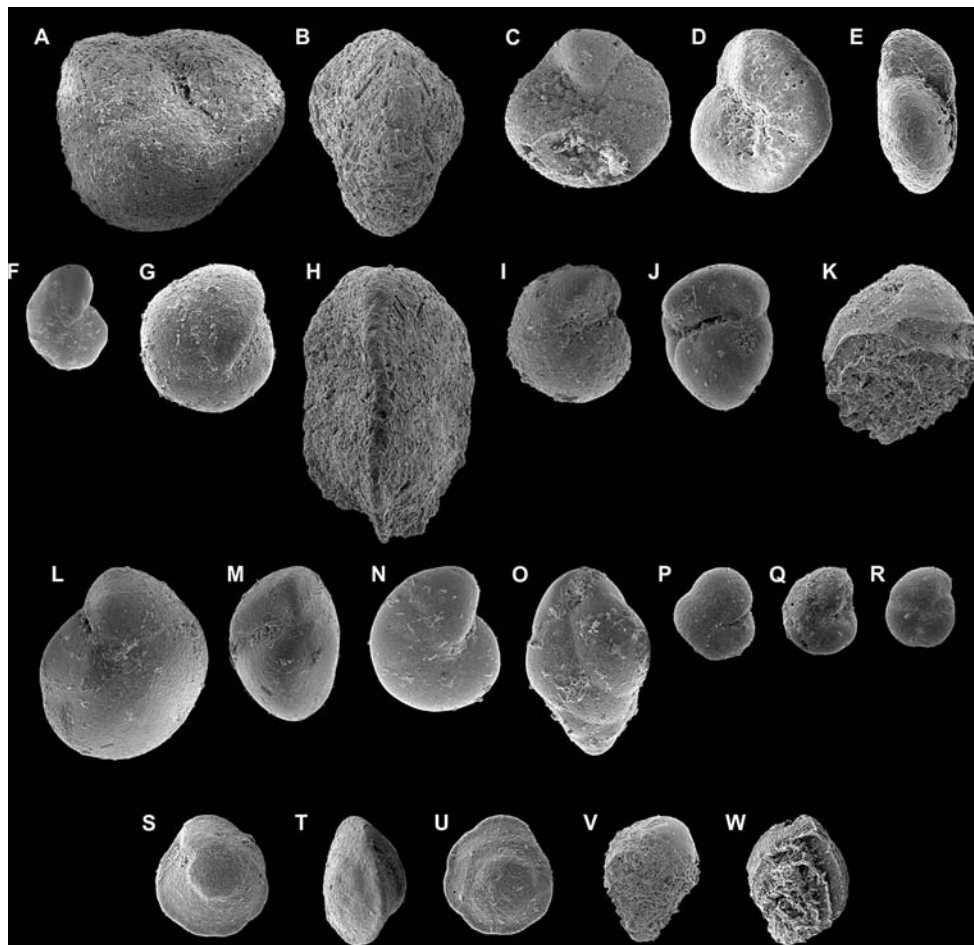
Fig. 5 Magnification: 1 cm = 100 μm. SEM micrographs of Paleocene and Eocene benthic foraminifera, Site 259. **a** *Dorothia* sp. (259-6R-6, 140–144 cm). **b** *Clavulinoides trilatera* (Cushman 1926) (259-6R-6, 120–124 cm). **c** *Paralabamina hillebrandti* (Fisher 1969): ventral view (259-6R-6, 120–124 cm). **d, e** *Stensonia beccariiformis* (White 1928): **d** ventral view, **e** side view (259-7R-3, 66–69 cm). **f** *Nonionella robusta* Plummer 1931; ventral view (259-6R-6, 120–124 cm). **g** *Pullenia coryelli* White 1929: ventral view (259-7R-1, 40–44 cm). **h** *Tritaxia havanensis* (Cushman & Bermudez 1937) (259-6R-6, 120–124 cm). **i, j.** *Gyroidinoides globosus* von Hagenow 1842: **i** ventral view, **j** side view (259-6R-6, 120–124 cm). **k** *Aragonia velascoensis* (Cushman 1925) (259-6R-6, 120–124 cm). **l, m** *Gyroidinoides beisseli* (White 1928): **l** ventral view, **m** side view (259-6R-6, 120–124 cm). **n** *Nonion havanense* Cushman & Bermudez 1937: ventral view (259-6R-6, 100–104 cm). **o** *Bulimina kugleri* Cushman & Renz 1942 (259-6R-6, 100–104 cm). **p** *Abyssamina quadrata* Schnitker & Tjalsma 1980: ventral view (259-6R-6, 112–115 cm). **q** *Anomalinoides spissiformis* (Cushman & Stainforth) 1945: ventral view (259-6R-6, 112–115 cm). **r** *Quadrimorphina profunda* Schnitker & Tjalsma 1980: ventral view (259-6R-6, 112–115 cm). **s, t, u** *Nuttallides truempyi* (Nuttall 1930): **s** ventral view, **t** side view, **u** spiral view (259-6R-6, 51–56 cm). **v** *Tappanina selmensis* (Cushman 1933), emend. Brotzen 1948 (259-6R-6, 100–104 cm). **w** *Aragonia aragonensis* (Nuttall 1930) (259-4R-5, 57–62 cm)

115 (55.17 mbsf). Across this interval, several cosmopolitan taxa have their LAD, including the calcareous foraminifera *Stensioeina beccariiformis*, *Pullenia coryelli*, *Gyroidinoides globosus* and *Buliminia thanetensis*, and the agglutinated foraminifera *Tritaxia havanensis* and *Clavulinoides* spp. (Table 3). As a consequence, there is a significant drop in the number of species identified per sample, or 'species richness' (Fig. 6). A prominent Benthic Foraminiferal Extinction Event (BFEE) coincides with the base of the CIE and P/E boundary at many locations (e.g., Thomas 1998).

Closely spaced samples across the BFEE at other locations reveal a short (~20 cm) 'post-extinction' interval where benthic foraminiferal assemblages are characterized by an extremely low diversity and the occurrence of very small, thin-walled tests (e.g., Thomas 1998). This succession is not found at Site 259, which may indicate an incomplete stratigraphic record near the onset of the IETM. Certainly, a short hiatus spans part of the IETM at other deep-sea sections, although it usually coincides with a clay layer (Bralower et al. 1997; Zachos et al. 2005), and typical post-

Table 3 Hancock et al. Paleogene CCD

Benthic Foraminifera

Sample	Depth (mbsf)	Preservation	Abyssamina poagi	Abyssamina quadrata	Alabamina creta	Alabamina dissonata	Alomorphina sp.	Anomalinoides globosus	Anomalinoides spissiformis	Anomalinoides sp.	Aragonia aragonensis	Aragonia velascoensis	Arenobulimina sp.	Bathysiphon sp.	Bolivinoides sp. (small)	Bulimina kugleri	Bulimina simplex	Bulimina thanetensis	Bulimina trinitatensis	Buliminella spp.	Chrysalogonium tenuicostatum	Cibicidoides hyphalus	Cibicidoides praemundulus	Cibicidoides pseudoperlucidus	Cibicidoides proprius	Cibicidoides velascoensis	Clavulinoides spp.	Clinapertina complanata	Clinapertina inflata	Clinapertina subplanispira	Ellipsoidina species	Bursenkoina sp.	Globocassidulina subglobosa	Gaudryina arenata	Gaudryina laevigata	Globobulimina sp.	Glomospira spp.	Gyroidinoides beisselli	Gyroidinoides globosus	Gyroidinoides quadratus	Gyroidinoides spp.	Heronallenia spp.
27-259-4R-5, 57-62	34.03	M-P	X	X				X	X	X	X		X			X						X		X				X	X	X			X								X	
27-259-5R-3, 61-66	38.61	M	X	X			X		X	X	X		X			X	X		X		X		X	X			X		X	X	X	X	X	X	X		X				X	X
27-259-6R-2, 120-124	49.25	M	X	X			X		X	X			X			X	X		X	X	X		X	X					X	X	X	X	X		X						X	X
27-259-6R-3, 100-104	50.55	P		X					X					X		X				X				X					X	X	X	X			X						X	
27-259-6R-4, 66-70	51.71	M	X	X					X	X				X		X					X			X						X	X	X	X									
27-259-6R-4, 140-144	52.45	M	X	X					X				X	X		X	X		X				X	X				X		X	X	X	X								X	X
27-259-6R-5, 100-104	53.55	M	X	X					X	X				X		X			X					X						X	X	X	X									
27-259-6R-5, 120-124	53.75	M	X	X					X	X				X		X								X						X	X	X	X								X	
27-259-6R-5, 140-144	53.95	M	X	X					X	X						X	X		X		X		X	X					X	X	X	X	X								X	
27-259-6R-6, 20-24	54.25	M	X	X					X	X						X	X							X						X	X	X	X									
27-259-6R-6, 40-44	54.45	M	X	X					X	X				X		X					X		X	X					X	X	X	X	X								X	X
27-259-6R-6, 51-56	54.56	M	X	X					X	X				X		X	X													X	X	X	X									
27-259-6R-6, 60-64	54.65	M	X	X					X							X								X					X	X	X	X	X									
27-259-6R-6, 80-84	54.85	M	X	X					X	X			X	X	X	X	X				X			X				X	X	X	X	X	X									
27-259-6R-6, 100-104	55.05	M	X	X					X	X			X	X		X						X							X	X	X	X	X								X	
27-259-6R-6, 112-115	55.17	M	X	X					X	X			X			X	X						X						X	X	X	X	X									
27-259-6R-6, 115-118	55.20	M		X	X				X			X				X		X				X	X				X		X	X	X	X						X	X		X	
27-259-6R-6, 120-124	55.25	M	X	X					X	X		X		X		X		X		X	X	X		X	X		X		X	X		X						X	X		X	
27-259-6R-6, 140-144	55.45	M	X	X			X		X	X		X			X	X		X	X	X		X		X	X		X		X	X	X	X	X					X	X			
27-259-7R-1, 20-24	55.70	M	X	X				X	X	X		X		X			X	X	X	X	X	X		X			X	X	X	X	X	X	X					X	X		X	X
27-259-7R-1, 40-44	55.90	M	X	X	X			X	X	X		X	X	X				X	X	X		X		X	X	X	X	X	X	X	X	X						X	X		X	
27-259-7R-1, 60-65	56.10	M	X	X		X		X	X	X		X					X	X	X	X		X		X		X	X	X	X	X	X		X		X			X	X	X	X	X
27-259-7R-1, 120-124	56.70	M	X	X				X	X									X		X		X					X	X	X	X			X					X	X			
27-259-7R-2, 62-65	57.62	M	X	X	X				X			X					X		X	X		X	X				X			X	X											
27-259-7R-2, 120-124	58.20	M	X					X				X						X	X	X		X	X	X			X	X	X		X							X	X		X	
27-259-7R-3, 66-69	59.16	M-G					X	X	X			X						X		X		X	X	X			X		X							X		X	X			
27-259-7R-3, 120-124	59.70	P-M						X	X									X		X		X	X				X		X									X	X			
27-259-7R-4, 52-57	60.52	P-B					X																				X															
27-259-7R-5, 51-56	62.01	M	X	X					X			X		X	X	X	X	X			X	X		X			X		X	X			X				X		X		X	X

Table 3 continued

Benthic Foraminifera — presence (X) / absence data by sample.

Sample	Depth (mbsf)
27-259-4R-5, 57-62	34.03
27-259-5R-3, 61-66	38.61
27-259-6R-2, 120-124	49.25
27-259-6R-3, 100-104	50.55
27-259-6R-4, 66-70	51.71
27-259-6R-4, 140-144	52.45
27-259-6R-5, 100-104	53.55
27-259-6R-5, 120-124	53.75
27-259-6R-5, 140-144	53.95
27-259-6R-6, 20-24	54.25
27-259-6R-6, 40-44	54.45
27-259-6R-6, 51-56	54.56
27-259-6R-6, 60-64	54.65
27-259-6R-6, 80-84	54.85
27-259-6R-6, 100-104	55.05
27-259-6R-6, 112-115	55.17
27-259-6R-6, 115-118	55.20
27-259-6R-6, 120-124	55.25
27-259-6R-6, 140-144	55.45
27-259-7R-1, 20-24	55.70
27-259-7R-1, 40-44	55.90
27-259-7R-1, 60-65	56.10
27-259-7R-1, 120-124	56.70
27-259-7R-2, 62-65	57.62
27-259-7R-2, 120-124	58.20
27-259-7R-3, 66-69	59.16
27-259-7R-3, 120-124	59.70
27-259-7R-4, 52-57	60.52
27-259-7R-5, 51-56	62.01

Taxa recorded (rows in original table):

sum taxa; Vaginulina sp.; uniloculor taxa; Turrilina brevispira; Tritaxia havanensis; Textularia sp.; Tappanina selmensis; Stensioeina beccariiformis; Spiroplectammina spectabilis; Siphotextularia spp.; Siphonodosaria pomuligera; Siphonodosaria lepidula; Siphonodosaria hispidula; Siphogenerinoides brevispinosa; Rhizammina epigona; Rhizammina spp.; Rectobulimina carpenterae; Quadrimorphina profunda; Pullenia jarvisi; Pullenia coryelli; pleurostomellid taxa; polymorphinid taxa; Paralabamina lunata; Paralabamina hillebrandti; Orthomorphina spp.; Oridorsalis umbonatus; Nuttallinella spp.; Nuttallinella floralis; Nuttallides truempyi; Nuttallides umbonifera; Nonionella sp.; Nonionella robusta; Nonion havanense; Nodosaria spp.; Neoflabellina semireticulata; Marssonella trochoides; Marssonella oxycona; Marginulina spp.; Lenticulina spp.; Laevidentalina, Dentalina spp.

Paleocene and Eocene benthic foraminiferal presence/absence data for Site 259. The BFEE is between 55.25 and 55.17 mbsf

Fig. 6 Benthic foraminiferal 'species richness' (sum of different taxa including genera and larger groups) and carbon isotope signatures of bulk sediment and *Nuttallides truempyi*, Site 259
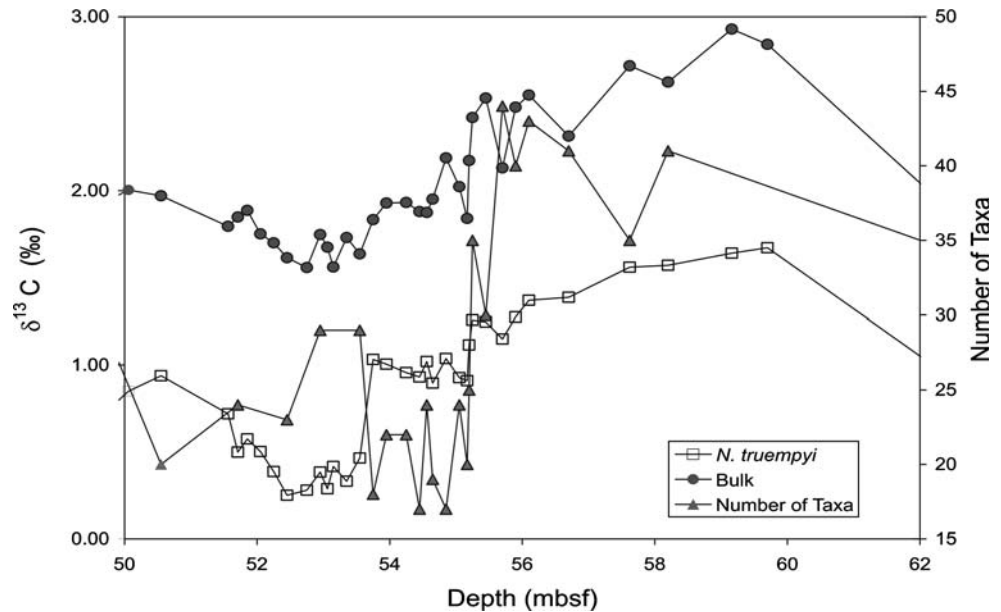
extinction assemblages have been recognized at all these sites. Post extinction faunas at Site 259 are dominated by abyssaminid species, *Quadrimorphina profunda* and *Nuttallides truempyi*, similar to post-extinction faunas found during the IETM at deep sites on Walvis Ridge (e.g., Thomas and Shackleton 1996; Zachos et al. 2004). If an interval is 'missing' at Site 259, it represents a short duration, probably <20 kyear (Thomas 1998).

Carbon isotopes

Bulk carbonate $\delta^{13}C$ varies from 1.23 to 2.93‰, showing a well-defined trend over the calcareous unit (Table 4; Figs. 3, 6). The $\delta^{13}C$ is distinctly high between 59.7 and 55.45 mbsf, where values range between 2 and 3‰. From 55.45 to 55.17 mbsf, and across the clay-rich horizon and BFEE, $\delta^{13}C$ declines by 0.69‰. Above a 1.62 m interval of relatively constant $\delta^{13}C$, values drop by another 0.28‰, and reach a minimum of 1.56‰ at 52.75 mbsf. Bulk carbonate $\delta^{13}C$ increases to 2.0‰ at 50.06 mbsf, and then generally decreases over the remainder of the sampled section, reaching a low of 1.23‰ at 33.36 mbsf (Table 4).

The $\delta^{13}C$ record of *Nuttallides truempyi* shows a broadly similar pattern to that of bulk carbonate across the calcareous unit, although values are generally lower by ~1‰ in the same samples (Table 4; Figs. 3, 6). Between 62.01 and 55.45 mbsf, $\delta^{13}C$ averages 1.5‰. A 0.35‰ drop in $\delta^{13}C$ to 0.91‰ then occurs from 55.45 to 55.17 mbsf. Above a 1.62 m interval of relatively constant $\delta^{13}C$, values drop again, from 1.03‰ at

53.57 mbsf to 0.47‰ at 53.55 mbsf. The 0.60‰ magnitude of this drop is noticeably greater than that in bulk carbonate. The $\delta^{13}C$ reaches a minimum of 0.28‰ at 52.75 mbsf, and then rises to 0.94‰ at 50.55 mbsf. Values remain relatively constant at an average of 0.5‰ for the remainder of the sampled section.

The $\delta^{13}C$ values of bulk carbonate presumably relate to the $\delta^{13}C$ of ΣCO_2 in surface waters, given that nannofossils dominate bulk sediment. The ~1‰ positive offset between bulk $\delta^{13}C$ and *Nuttallides truempyi* $\delta^{13}C$, therefore, may reflect the carbon isotope gradient in the water column (Corfield 1994).

Non-carbonate mineralogy

All six samples analyzed for their carbonate-free mineralogy have similar XRD traces (Table 5; Fig. 7). Minerals identified include expanding clays, quartz, heulandite (zeolite), pyrolusite, feldspars, and mica. Traces of residual calcite were also detected. Similar minerals were identified in the few previously examined sediment samples from Site 259 (Cook et al. 1974). The results suggest that the non-carbonate fraction of sediment remained the same before, during and after deposition of the calcareous unit.

Discussion

A plug of carbonate sediment occurs between 35 and 57 mbsf at Site 259 (Fig. 3). Sediment within this interval generally has between 50 and 80% calcium

Table 4 Hancock et al. Paleogene CCD

Sample: leg, core, section, interval (cm)	Depth (mbsf)	*N. truempyi* δ^{13}C	*N. truempyi* δ^{18}O	Bulk δ^{13}C	Bulk δ^{18}O
27-259-3R-2, 110–116	20.10	–	–	–	–
27-259-4R-1, 60–65	28.06	–	–	–	–
27-259-4R-2, 100–105	29.96	0.96	–0.76	–	–
27-259-4R-3, 22–26	30.68	0.42	–0.77	–	–
27-259-4R-4, 60-65	32.56	–	–	–	–
27-259-4R-4, 140–144	33.36	0.23	–0.78	1.23	–0.87
27-259-4R-5, 57–62	34.03	0.31	–0.78	–	–
27-259-4R-6, 61–66	35.57	0.30	–0.49	1.58	–0.89
27-259-4R-6, 120–124	36.16	0.46	–0.43	1.65	–0.75
27-259-5R-1, 103–108	37.53	0.14	0.68	–	–
27-259-5R-2, 61–66	38.61	0.38	–0.66	1.53	–0.65
27-259-5R-2, 120–124	39.20	0.14	–0.65	1.67	–0.54
27-259-5R-3, 61–66	40.11	0.48	–0.53	1.58	–0.72
27-259-5R-3, 120–124	40.70	0.31	–0.59	1.45	–0.97
27-259-5R-4, 61–66	41.61	0.37	–0.54	1.59	–0.76
27-259-5R-4, 120–124	42.20	0.37	–0.52	1.43	–0.92
27-259-5R-5, 56–61	43.06	0.83	–0.31	1.97	–0.64
27-259-5R-5, 120–124	43.70	0.90	–0.42	1.95	–0.60
27-259-6R-1, 51–56	47.06	0.43	–0.63	1.60	–0.86
27-259-6R-1, 120–124	47.75	0.39	–0.57	1.65	–0.60
27-259-6R-2, 51–56	48.56	0.58	–0.51	1.78	–0.61
27-259-6R-2, 120–124	49.25	0.57	–0.41	1.85	–0.78
27-259-6R-3, 51–56	50.06	0.85	–0.27	2.00	–0.66
27-259-6R-3, 100–104	50.55	0.94	–0.32	1.97	–0.54
27-259-6R-4, 51–56	51.56	0.72	–0.30	1.80	–0.60
27-259-6R-4, 66–70	51.71	0.50	–0.52	1.85	–0.65
27-259-6R-4, 80–84	51.85	0.58	–0.47	1.89	–0.53
27-259-6R-4, 100–104	52.05	0.50	–0.46	1.75	–0.69
27-259-6R-4, 120–124	52.25	0.39	–0.55	1.70	–0.72
27-259-6R-4, 140–144	52.45	0.25	–0.61	1.61	–0.76
27-259-6R-5, 20–24	52.75	0.28	–0.57	1.56	–0.83
27-259-6R-5, 51–56	53.06	0.29	–0.70	1.68	–0.65
27-259-6R-5, 60–64	53.15	0.42	–0.66	1.56	–0.68
27-259-6R-5, 80–84	53.35	0.33	–0.64	1.73	–0.60
27-259-6R-5, 100–104	53.55	0.47	–0.64	1.64	–0.71
27-259-6R-5, 120–124	53.75	1.03	–0.55	1.83	–0.84
27-259-6R-5, 140–144	53.95	1.01	–0.53	1.93	–0.94
27-259-6R-6, 20–24	54.25	0.96	–0.56	1.93	–0.87
27-259-6R-6, 40–44	54.45	0.93	–0.46	1.88	–0.98
27-259-6R-6, 51–56	54.56	1.02	–0.50	1.87	–0.90
27-259-6R-6, 60–64	54.65	0.90	–0.59	1.95	–0.78
27-259-6R-6, 80–84	54.85	1.04	–0.48	2.19	–0.96
27-259-6R-6, 100–104	55.05	0.93	–0.44	2.02	–0.72
27-259-6R-6, 112–115	*55.17*	*0.91*	*–0.35*	*1.84*	*–0.68*
27-259-6R-6, 115–118	*55.20*	*1.12*	*–0.36*	*2.17*	*–0.96*
27-259-6R-6, 120–124	*55.25*	*1.26*	*–0.35*	*2.42*	*–0.85*
27-259-6R-6, 140–144	55.45	1.25	–0.14	2.53	–0.37
27-259-7R-1, 20–24	55.70	1.15	–0.39	2.13	–0.87
27-259-7R-1, 40–44	55.90	1.28	–0.23	2.48	–0.51
27-259-7R-1, 60–65	56.10	1.37	–0.06	2.55	–0.42
27-259-7R-1, 120–124	56.70	1.39	–0.14	2.31	–0.80
27-259-7R-2, 62–65	57.62	1.56	–0.08	2.72	–0.32
27-259-7R-2, 120–124	58.20	1.57	–0.15	2.62	–0.99
27-259-7R-3, 66–69	59.16	1.64	–0.20	2.93	–0.60
27-259-7R-3, 120–124	59.70	1.67	–0.09	2.84	–0.85
27-259-7R-4, 52–57	60.52	–	–	–	–
27-259-7R-4, 116–120	61.16	–	–	–	–
27-259-7R-5, 51–56	62.01	1.05	–0.56	2.04	–1.03
27-259-8R-1, 80–85	65.80	–	–	–	–

Bulk carbonate and *Nuttallides truempyi* carbon and oxygen isotopes, Site 259. IETM interval is in italics

Table 5 Hancock et al. Paleogene CCD

Sample: leg, core, section, interval (cm)	Depth (mbsf)	Mineral
27-259-4R-3, 17–21	30.63	Expanding clay, quartz, feldspar, heulandite, pyrolusite
27-259-4R-3, 41–44	30.87	Expanding clay, quartz, feldspar, heulandite, pyrolusite
27-259-5R-3, 120–124	40.70	Expanding clay, quartz; feldspar, heulandite, mica
27-259-6R-2, 120–124	49.25	Expanding clay, quartz, feldspar, heulandite, pyrolusite, mica
27-259-7R-4, 116–120	61.16	Expanding clay, quartz, feldspar, heulandite, pyrolusite
27-259-7R-5, 120–124	62.70	Expanding clay, quartz, heulandite, pyrolusite

Mineralogy from powder X-ray diffraction analysis for samples below, within and above the carbonate interval

carbonate, and never drops below 37% in bulk 10 cm^3 samples. Most of this carbonate consists of nannofossils, demonstrating a dominantly pelagic origin.

Although planktic foraminifera are generally rare and poorly preserved, their assemblages indicate that the calcareous interval was deposited between about 57 and 52 Ma (Fig. 3). Carbon isotope curves constructed from bulk carbonate and *Nuttallides truempyi* exhibit trends that support this timing (Fig. 1). Sediment deposited between 62.01 and 55.45 mbsf has foraminiferal assemblages and relatively high δ^{13}C consistent with Zone P4c and the latter part of the PCIM. Sediment deposited around 55.2 mbsf has an unusual planktic foraminiferal assemblage with large *Acarinina*, a prominent BFEE, and a drop in δ^{13}C consistent with the early stages of the IETM. However, the magnitude of the δ^{13}C drop is not as great as the CIE observed at other locations (e.g., Kennett and Stott 1991; Thomas and Shackleton 1996; Bralower et al. 1997; Katz et al. 1999; Zachos et al. 2005). Sediment deposited between 55.2 and ~50 mbsf has foraminiferal assemblages and a δ^{13}C excursion consistent with the IETM and the main CIE in the latter stage of Zone P5, and the subsequent recovery into Subzone P6a, although this correlation is potentially problematic as discussed below. Sediment deposited from ~50 to 30 mbsf has foraminiferal assemblages and declining, relatively low δ^{13}C values consistent with Zone P6b, and the drop in δ^{13}C heading into the EECO.

The 31 m thick upper Paleocene–lower Eocene calcareous unit was deposited relatively slowly, accumulating at an average rate of 0.6 cm/kyear. This rate is probably close to the original rate of deposition because the overlying sediment cover is only 29 m thick so that compaction has been minimal. Slow deposition is consistent with the yellowish orange colour and the presence of pyrolusite (MnO_2), which together support a low flux of organic carbon and oxidizing conditions during accumulation. Benthic foraminiferal assemblages also indicate an oxygenated environment and oligotrophic conditions.

Calcareous sediment at Site 259 was deposited above the CCD but within the lower part of the lyso-cline. Modern open-ocean locations within this depth interval typically have carbonate contents <70% and sedimentation rates <2 cm/year because the relative burial fluxes of biogenic carbonate are similar to those of background terrigenous aluminosilicate phases (Kennett 1982). These sites, like the Paleogene sediment at Site 259, are also characterized by impoverished planktic foraminiferal assemblages dominated by thick-walled species and high ratios of benthic to planktic foraminifera (e.g., Berger 1968; Thunell 1976; Williams et al. 1985a, b). Deep-sea sediment deposited at high latitudes and above the lysocline often has planktic foraminiferal assemblages characterized by low diversity but high relative abundances (Stott and Kennett 1990; Huber 1991). The paleolocation of Site 259 may, therefore, have contributed to the low diversity. However, it is difficult to explain the low abundances of planktic foraminifera without differential dissolution.

Site 259 lay beneath 4,000 m of water during the early Paleogene, given the age and composition of basement, and assumptions regarding initial ridge height and thermal subsidence (van Andel 1975). Such a depth cannot be rigorously supported with data from our study, although the benthic foraminiferal assemblages are consistent with an abyssal depth during the Paleocene and Eocene (Thomas 1998). Irrespective of the absolute paleodepth, the calcareous interval overlies and underlies carbonate-free zeolitic claystones. There is no evidence for regional tectonism that would have raised the seafloor of Perth Abyssal Plain in the early Paleogene (Muller et al. 2000). Thus, either some depositional process (e.g., gravity flows) led to preferential accumulation of carbonate-rich sediment during this time, or the CCD dropped between ~57 and 52 Ma.

The occurrence of silt, large quartz grains and the wide size variance in benthic foraminifera species suggest that downslope transport, perhaps by turbidity currents, has contributed some material to almost all samples. Given such evidence, one might suggest that the latest Paleocene and earliest Eocene was a time of enhanced delivery of sediment, including carbonate,
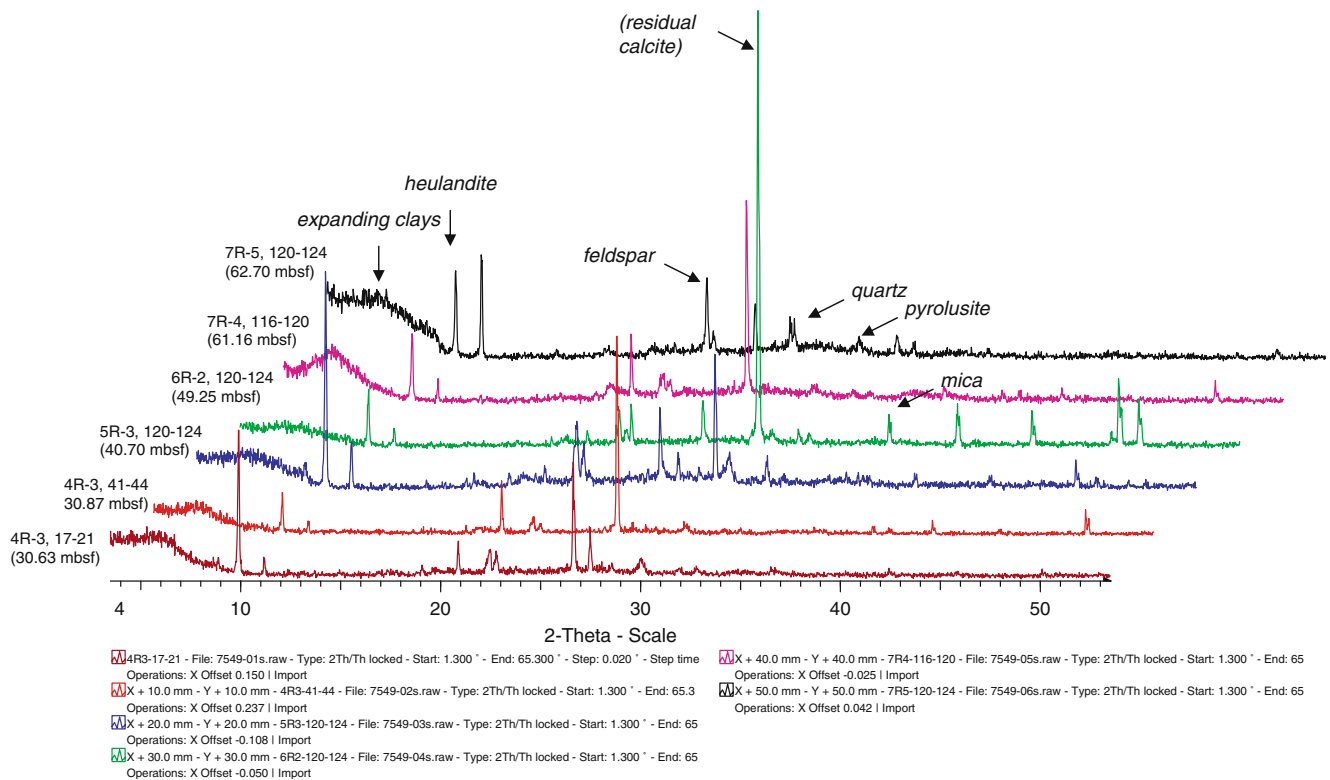
Fig. 7 Powder X-ray diffraction analyses of selected samples from Site 259. Two samples are taken from the clay below the carbonate interval, two samples from within the carbonate interval, and two samples from overlying clays

from shallower locations to Site 259. Here we emphasise the overall pelagic composition (with the exception of these large quartz grains) and stratigraphic continuity of the section. With the possible exception of some repeated sediment intervals (Proto-Decima 1974), all stratigraphic indicators, including nannofossil assemblages, planktic and benthic foraminiferal assemblages, and carbon isotope variations occur in a systematic and expected order. Moreover, the non-carbonate fraction of sediment has a similar mineralogical composition before, during, and after the calcareous interval. This suggests similar sediment provenance and transport throughout the early Paleogene. Overall, the lithological record at Site 259 supports a relatively deep CCD between ~57 and 52 Ma.

The carbonate plug at Site 259 correlates in time with an upper Paleocene–lower Eocene interval of enhanced carbonate preservation at other locations (Fig. 8). ODP sites 1262 and 1267 lie at 4759 and 4356 mbsl depth on Walvis Ridge in the southeast Atlantic Ocean (Zachos et al. 2004, 2005). Calcium carbonate contents are unusally high (>80%) at these sites for sediment deposited from ~57 to 51 Ma (Fig. 8), except across the IETM (Shipboard Scientific Party 2004; Zachos et al. 2005). These high carbonate contents were interpreted by Zachos et al. (2004) to

reflect a late Paleocene–early Eocene lowering of the CCD and lysocline (Fig. 9). ODP sites 1209 and 1211 lie at 2387 and 2907 mbsl on Shatsky Rise in the west central Pacific Ocean (Bralower et al. 2002). An interval of high carbonate content and enhanced carbonate preservation occurred from ~57 to 51 Ma (Fig. 8), again with the exception of the IETM (Hancock and Dickens 2005). This trend has been interpreted as a lowering of the lysocline (Hancock and Dickens 2005). ODP Site 766 lies at 3,998 mbsl on Gascoyne Abyssal Plain off northwest Australia (Fig. 2). This site, probably at ~3,500 m water depth during the late Paleocene (Shipboard Scientific Party 1990) (Fig. 9), contains a ~45 m thick calcareous unit deposited between ~57 to 51 Ma (Fig. 8). Similar to Site 259, a major hiatus occurs at the upper boundary of this interval, spanning from the upper lower Eocene to lowermost Pliocene. Sediment from the middle Paleocene is also missing (Shipboard Scientific Party 1990).

Established CCD compilations (Berger and von Rad 1972; van Andel 1975) indicate a relatively shallow (~3,500 m) and unchanging CCD in all oceans between 60 and 50 Ma, inconsistent with the lithological records at Site 259 and other locations (Fig. 8). We suggest the CCD dropped between nominally ~57 and 52 Ma at

multiple locations, although the magnitude of this shift cannot be determined with available information. This interpretation, if correct, raises two issues.

ODP Leg 199 drilled six sites (1215, 1217, 1219–1222) on the eastern distal flank of East Pacific Rise that terminate in uppermost Paleocene mid-ocean ridge basalt (Lyle et al. 2002). Using the records at these sites, Rea and Lyle (2005) presented an Equatorial Pacific CCD curve beginning ca. 56.5 Ma that shows a shallow (~3,200 m) and generally invariant CCD from this age to 42 Ma. However, the ''flat'' late Paleocene–early Eocene portion of their curve is not supported by data. The Leg 199 sites contain a succession of upper Paleocene basalt, upper Paleocene–lower Eocene calcareous chalk, and lower Eocene carbonate-free sediment, with the second transition marking when the sites dropped below the CCD (Lyle et al. 2002; Rea and Lyle 2005). Rea and Lyle (2005) indicate an age of 53.4–53 Ma for the second transition, which would suggest a shallow CCD at this time in conflict with our interpretation. In fact, however, the transition occurs in a >5 m coring gap at Sites 1219 and 1220, so that the age estimate (determined by nannofossils below the gap) is a maximum. Cores at Site 1215, which were not used by Rea and Lyle (2005) to construct their CCD curve, show instead that the transition occurs some 2–3 m above the FAD of *Discoaster lodoensis* (Lyle et al. 2002), which has been dated at 52.4 Ma (Fig. 8). We also point out that, given the similarity of basement ages for the sites (56.5–55.0 Ma; Lyle et al. 2002), the depth trajectory of the CCD before the timing of the second transition is entirely conjectural. In short, the sediment records recovered by Leg 199 do not discount a CCD that was relatively deep in the late Paleocene and early Eocene and rose past 3,200–3,300 mbsl around 52 Ma.

A significant lowering of the CCD at multiple, widespread locations between ~57 and 52–51 Ma necessitates a mechanism. At present, it is difficult to gauge whether the CCD drop occurred only in certain regions, notably portions of the south Atlantic, south Indian and Pacific oceans, or whether it occurred globally. In the first case, the lowered CCD might signify a change in the flow of deep ocean water. Specifically, waters bathing the seafloor at southern latitudes and in the Pacific could have become younger and less corrosive to calcium carbonate. Benthic foraminiferal carbon isotope records may support this interpretation, as they suggest a decrease in the $\delta^{13}C$ gradient between sites in the Atlantic and Pacific during the late Paleocene and the early Eocene (Corfield 1994). If the CCD drop was global, however, it might instead signify changes in ocean chemistry and
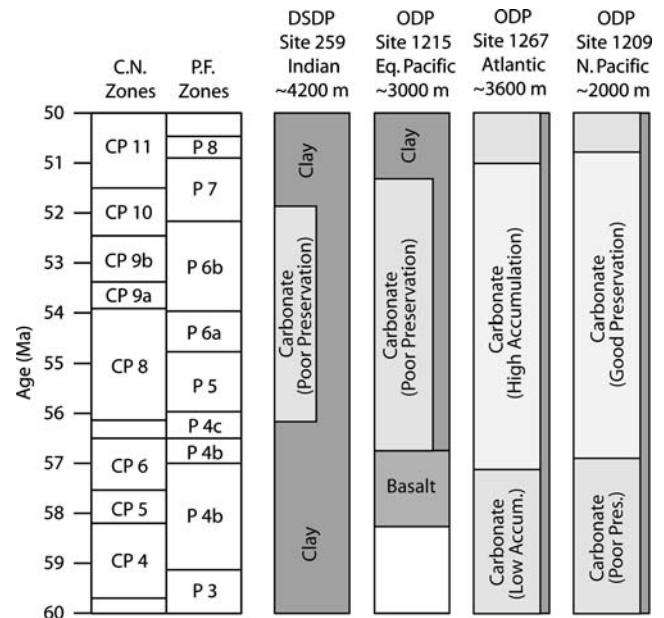

Fig. 8 Upper Paleocene–Lower Eocene lithologic logs at four sites discussed in this study and listed with approximate average paleodepth. The logs highlight the carbonate content and its preservation (poor/good) or accumulation (low/high). The time scale is from Berggren et al. (1995) as modified in later works (see Lyle et al. 2002; Zachos et al. 2004). Carbonate data come from the following sources: Site 259 (this study); Site 1215 (Lyle et al. 2002); Site 1262 (Zachos et al. 2004); Site 1209 (Hancock et al. 2005). Note that lithologic changes across short-term events (e.g., the IETM) are not shown

higher concentrations of CO_3^{2-} or Ca^{2+}. Enhanced carbonate accumulation at Site 259 and elsewhere (Figs. 8, 9) roughly coincided with the long-term warming and decrease in $\delta^{13}C$ from the late Paleocene through the early Eocene (Fig. 1). It is possible that this was a time of enhanced chemical weathering and greater inputs of dissolved CO_3^{2-} and Ca^{2+} to the ocean.

The massive input of carbon heralding the IETM should have caused extensive dissolution of carbonate on the seafloor, with the location and magnitude of dissolution relating to the source and mass of the carbon injection (Dickens et al. 1997; Dickens 2000; Zachos et al. 2005). In several deep-sea sections, notably from sites in the central and north Atlantic Ocean, pronounced dissolution of carbonate indeed marks the base of the IETM (e.g., Bralower et al. 1997; Zachos et al. 2005).

Within this context, the ~5 m-thick, calcareous section across the IETM at Site 259 is intriguing but difficult to interpret. On the one hand, the section displays features consistent with an expanded record: it lacks a prominent clay layer, and it accumulated at a significantly higher rate than sediment deposited earlier and later. Bulk carbonate and *Nuttallides* also display a stepped drop in $\delta^{13}C$ at the start of the CIE

Fig. 9 Carbonate (wt%) from Walvis Ridge sites (adapted from Zachos et al. 2004, Fig. 45). Subsidence curves for DSDP Site 259 (adapted from van Andel 1975) and ODP Site 766 (adapted from Shipboard Scientific Party 1990, Fig. 28) are also plotted. The *white line* represents carbonate deposition, and the *dashed line* when little or no carbonate was deposited
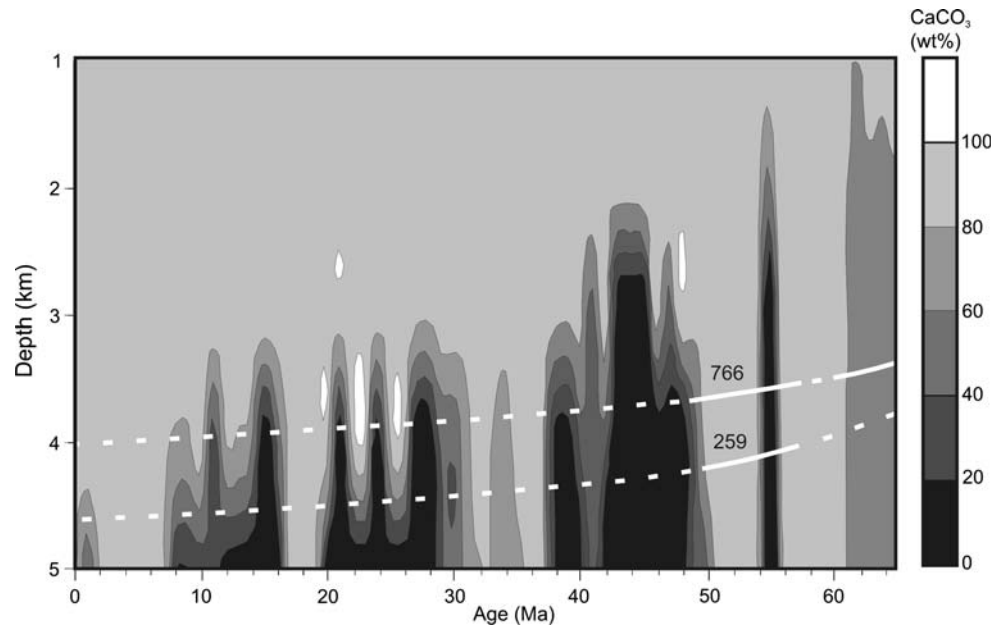
(Fig. 3), a feature seen in expanded IETM records at other locations (e.g., Ocean Drilling Program Site 690, Bains et al. 1999). Thus, in stark contrast to sites from the Atlantic Ocean, the record at Site 259 seems to suggest that carbonate dissolution was not very intense in deep waters of the southeastern Indian Ocean during the ITEM. On the other hand, the "post-extinction" benthic foraminiferal assemblage is missing, and the magnitude of the CIE is reduced compared to many other sites. This may signify that, despite an expanded record across the IETM, the initial part of the event is missing.

Conclusions

1. The ~31 m-thick upper Paleocene–lower Eocene calcareous unit at DSDP Site 259 generally comprises sediment with >50 wt% carbonate. The carbonate fraction is dominated by relatively dissolution-resistant nannofossil and foraminifera tests, particularly benthic foraminifera. The remaining sedimentary components, mostly clays and quartz, are similar to those deposited below and above the calcareous unit.
2. Though rare, planktic foraminifera indicate that the calcareous unit corresponds to zones P4c through P6b (~57–52 Ma). Carbon isotope records at Site 259, constructed using bulk carbonate and *Nuttallides*, show a characteristic series of changes consistent with this depositional age, as are the benthic foraminiferal assemblages.
3. Tectonic reconstructions indicate that Site 259 probably lay at >4,000 m water depth during the late Paleocene and early Eocene. The calcareous interval, therefore, suggests a relatively deep CCD between 57–52 Ma not previously recognized in Cenozoic CCD reconstructions. Sediment records at other deep-sea sites support the interpretation that the CCD was deep over a 5–6 myear interval in the late Paleocene–early Eocene.
4. The long-term drop in the CCD roughly coincided with a long-term warming and decrease in $\delta^{13}C$. It is possible that this was a time of enhanced weathering and fluxes of CO_3^{2-} and Ca^{2+}.
5. The IETM is recognized at Site 259 by a clear BFEE, a negative excursion in $\delta^{13}C$, and a rapid influx in large *Acarinina*. However, the stratigraphic record across the event is difficult to understand within the context of information at other locations. Given the inferred abyssal water depth of Site 259 and the pronounced dissolution of carbonate observed at other locations across the IETM, we would have expected a highly condensed record, but the sedimentary record of the IETM at Site 259 appears to be expanded.

Appendix 1. Taxonomic list of Paleocene and Eocene calcareous foraminifera, Site 259

Planktic foraminifera

Acarinina coalingensis (Cushman & Hanna 1927)
Acarinina mckannai (White, 1928)
Acarinina nitida (Martin 1943)
Acarinina primitiva (Finlay 1947)
Acarinina soldadoensis (Bronnimann 1952)
Acarinina subsphaerica (Subbotina 1947)
Acarinina wilcoxensis (Cushman & Ponton, 1932)
Chiloguembelina crinita (Glaessner 1937)
Chiloguembelina wilcoxensis (Cushman & Ponton 1932)
Globigerinatheka senni (Beckmann 1953)
Subbotina velascoensis (Cushman 1925)
Morozovella lensiformis (Subbotina 1953)
Morozovella subbotinae (Morozova 1939)
Zeauvigerina zealandica (Finlay 1939)

Benthic foraminifera

Abyssamina poagi (Schnitker & Tjalsma 1980)
Abyssamina quadrata (Schnitker & Tjalsma 1980)
Alabamina creta (Finlay 1940)
Alabamina dissonata (Cushman & Renz 1948)
Allomorphina sp.
Anomalinoides globosus (Brotzen 1945)
Anomalinoides spissiformis (Cushman & Stainforth 1945)
Anomalinoides sp.
Aragonia aragonensis (Nuttall 1930)
Aragonia velascoensis (Cushman 1925)
Arenobulimina sp.
Bathysiphon sp.
Bolivinoides sp.
Bulimina kugleri (Cushman & Renz 1942)
Bulimina simplex (Terquem 1882)
Bulimina thanetensis (Cushman & Parker 1947, emend. Haynes 1954)
Bulimina trinitatensis (Cushman & Jarvis 1928)
Buliminella spp.
Chrysalogonium tenuicostatum (Cushman & Bermudez 1936)
Cibidoides hyphalus (Fisher 1969)
Cibicidoies praemundulus (Berggren & Miller 1986)
Cibicidoides pseudoperlucidus (Bykova 1954)
Cibicidoides proprius (Brotzen 1948)
Cibicidoides velascoensis (Cushman 1925)
Clavulinoides sp.
Clavulinoides trilatera (Cushman 1926)NOTE: trilateral, not trilateral

Clinapertina complanata (Tjalsma & Lohmann 1983)
Clinapertina inflata (Tjalsma & Lohmann 1983)
Clinapertina subplanispira (Tjalsma & Lohmann 1983)
Ellipsoidina spp.
Fursenkoina sp.
Globocassidulina subglobosa (Brady 1881)
Gaudryina arenata (Cushman 1936)
Gaudryina laevigata (Franke 1914)
Globobulimina sp.
Glomospira spp.
Gyroidinoides beisseli (White 1928)
Gyroidinoides globosus (von Hagenow 1842)
Gyroidinoides quadratus (Cushman & Church 1929)
Gyroidinoides spp.
Heronallenia spp.
Laevidentalina, Dentalina spp.
Lenticulina spp.
Marginulina spp.
Marssonella oxycona (Reuss 1860)
Marssonella trochoides (d'Orbigny 1852)
Neoflabellina semireticulata (Cushman & Jarvis 1928)
Nodosaria spp.
Nonion havanense (Cushman & Bermudez 1937)
Nonionella robusta (Plummer 1931)
Nonionella sp.
Nuttallides umbonifera (Cushman 1933)
Nuttallides truempyi (Nuttall 1930)
Nuttallinella florealis (White 1928)
Nuttallinella sp.
Oridorsalis umbonatus (Reuss 1851)
Orthomorphina spp.
Paralabamina hillebrandti (Fisher 1969) (=Eponides whitei von Hillebrandt 1962)
Paralabamina lunata (Brotzen 1948)
Polymorphinid taxa
Pleurostomellid taxa
Pullenia coryelli (White 1929)
Pullenia jarvisi (Cushman 1936)
Pyramidina rudita (Cushman & Parker 1936)
Quadrimorphina profunda (Schnitker & Tjalsma 1980)
Rectobulimina carpentierae (Marie 1956)
Rhizammina sp.
Rhzehakina epigona (Rjzehak 1895)
Siphogenerinoides brevispinosa (Cushman 1939)
Siphonodosaria hispidula (Cushman 1917)
Siphonodosaria lepidula
Siphonodosaria pomuligera (Stache 1865)
Siphotextularia sp.
Spiroplectammina spectabilis (Grzybowski 1898)

Stensioeina beccariiformis (White 1928)

Tappanina selmensis (Cushman 1933), emend. Brotzen 1948

Textularia sp.

Tritaxia havanensis (Cushman & Bermudez 1937)

Turrilina brevispira (ten Dam 1944)

Unilocular taxa

Vaginulina spp.

References

Alegret L, Thomas E (2001) Upper Cretaceous and lower Paleogene benthic foraminifera from northeastern Mexico. Micropaleontology 47:269–316

Archer DE, Maier-Reimer E (1994) Effect of deep-sea sedimentary calcite preservation on atmospheric CO_2 concentration. Nature 367:260–263

Aubry MP, Berggren W et al (2003) Chronostratigraphic terminology at the Paleocene/Eocene boundary. In: Wing SL, Gingerich PD, Schmitz B et al (eds) Causes and consequences of the globally warm climates in the early Paleogene. The Geological Society of America, Spec. Paper 369, pp 551–566

Bains S, Corfield RM et al (1999) Mechanisms of climate warming at the end of the Paleocene. Science 285:724–727

Berger WH (1968) Planktonic foraminifera; selective solution and paleoclimatic interpretation. Deep-Sea Res Oceanograph Abstracts 15:31–43

Berger WH, Adelseck CG et al (1976) Distribution of carbonate in surface sediments of the Pacific Ocean. J Geophys Res 81:2617–2627

Berger WH, von Rad U (1972) Cretaceous and Cenozoic sediments from the Atlantic Ocean Init. Repts. DSDP, 14: Washington US Government Printing Office, pp 787–886

Berggren WA, Kent DV et al (1995) A revised Cenozoic geochronology and chronostratigraphy. In: Berggren WA, Kent DV, Aubry MP et al (eds) Geochronology, time scales and global stratigraphic correlation, SEPM Special Publication 54, pp 129–212

Bode GW (1974) Carbon and carbonate analyses, Leg 27. In: Heirtzler JR, Veevers JJ, Bolli HM et al (eds) Init. Repts. DSDP, 27: Washington US Government Printing Office, pp 499–505

Bolli HM, Beckmann JP et al (1994) Benthic foraminiferal biostratigraphy of the South Caribbean Region. Cambridge University Press, Cambridge, p 408

Bralower TJ, Premoli Silva I et al (2002) Proc. ODP, Init. Repts, 198 [CD-ROM]. Available from: Ocean Drilling Program, Texas A&M University, College Station, TX 77845–9547, USA

Bralower TJ, Rohl U et al (1997) High-resolution records of the late Paleocene thermal maximum and circum-Caribbean volcanism: is there a causal link? Geology 11:963–966

Cook HE, Zemmels I et al (1974) X-ray mineralogy data, eastern Indian Ocean—Leg 27 Deep Sea Drilling Project. In: Heirtzler JR, Veevers JJ, Bolli HM (eds) Init. Repts. DSDP, 27: Washington US Government Printing Office, pp 535–548

Corfield RM (1994) Palaeocene oceans and climate; an isotopic perspective. Earth-Sci Rev 37:225–252

Cramer BS, Wright AA et al (2003) Orbital climate forcing of $\delta^{13}C$ excursions in the late Paleocene–early Eocene (chrons C24n–C25n). Paleoceanography 18(4):1097

Dickens GR (2000) Methane oxidation during the late Palaeocene thermal maximum. Bull Soc Geologique France 171:37–49

Dickens GR, Castillo MM et al (1997) A blast of gas in the latest Paleocene; simulating first-order effects of massive dissociation of oceanic methane hydrate. Geology 25:259–262

Dupuis C, Aubry MP et al (2003) The Dababiya Quarry section: lithostratigraphy, clay mineralogy, geochemistry and paleontolgoy. Micropaleontology 49:41–59

Hancock HJL, Chaproniere GC et al (2002) Early Palaeogene planktic foraminiferal and carbon isotope stratigraphy, Hole 762C, Exmouth Plateau, northwest Australian margin. J Micropalaeontol 21:29–42

Hancock HJL, Dickens GR (20050 Carbonate dissolution episodes in Paleocene and Eocene sediment, Shatsky Rise, west-central Pacific. In: Bralower TJ, Premoli Silva I, Malone MJ (eds) Proceedings of ODP, science results, 198 [Online]. Available from World Wide Web: <http://www-odp.tamu.edu/publications/198_SR/116/116.htm>. [Cited 2005–09-04]

Hancock HJL, Dickens GR et al (2003) Foraminiferal and carbon isotope stratigraphy through the Paleocene–Eocene transition at Dee Stream, Marlborough, New Zealand. N Z J Geol Geophy 46:1–19

Hollis CJ, Dickens GR et al (2005) The Paleocene–Eocene transition at Mead Stream, New Zealand: a southern Pacific record of early Cenozoic global change. Palaeogeogr Palaeoclimatol Palaeoecol 215:313–343

Huber BT (1991) Paleogene and early Neogene planktonic foraminifer biostratigraphy of sites 738 and 744, Kerguelen Plateau (southern Indian Ocean). Proc Ocean Drilling Program Sci Results 119:427–449

Katz ME, Pak DK et al (1999) The source and fate of massive carbon input druing the latest Paleocene thermal maximum. Science 286:1531–1533

Katz ME, Wright JD et al (2003) Early Cenozoic benthic foraminiferal isotopes: species reliability and interspecies correction factors. Paleoceanography 18(2):1024. DOI 10.1029/2002PA000798

Katz ME, Wright JD et al (2005) Biological overprint of the geological carbon cycle. Mar Geol 217:323–338

Kelly DC (2002) Response of Antarctic (ODP Site 690) planktonic foraminifera to the Paleocene–Eocene thermal maximum; faunal evidence for ocean/climate change. Paleoceanography 17(4):1071. DOI 10.1029/2002PA000761

Kennett JP (1982) Marine geology. Prentice-Hall, Englewood Cliffs, p 813

Kennett JP, Stott L (1991) Abrupt deep-sea warming, palaeoceanographic changes and benthic extinctions at the end of the Paleocene. Nature 353:225–229

Krasheninnikov GF (1974) Cretaceous and Paleogene planktonic foraminifera, Leg 27 of the Deep Sea Drilling Project. In: Heirtzler JR, Veevers JJ, Bolli HM (eds) Init. Repts. DSDP, 27: Washington US Government Printing Office, pp 663–671

Kump LR, Arthur MA (1999) Interpreting carbon-isotope excursions; carbonates and organic matter. Chem Geol 161:181–198

Kurtz A, Kump LR et al (2003) Early Cenozoic decoupling of the global carbon and sulfur cycles. Paleoceanography 18(4):1090. DOI 10.1029/2003PA000908

Loeblich AR Jr, Tappan HN (1988) Foraminiferal genera and their classification. Von Nostrand and Reinhold Company, New York, p 970

Lourens L, Sluijs A et al (2005) Astronomical modulation of late Palaeocene to early Eocene global warming events. Nature 435:1083–1087

Lyle MW, Wilson PA et al (2002) Proc. ODP Init. Repts., 199 [CD-ROM]. Available from: Ocean Drilling Program, Texas A&M University, College Station TX 77845–9547, USA

Mekik FA, Loubere PW et al (2002) Organic carbon flux and organic carbon to calcite flux ratio recorded in deep-sea carbonates: demonstration and a new proxy. Global Biogeochem Cycles 16:1–15

Mueller G, Gastner M (1971) The "Karbonate-Bombe", a simple device for the determination of the carbonate content in sediments, soils, and other materials. Neues Jahrbuch fuer Mineralogie Monatshefte 10:466–469

Muller RD, Gaina C et al (2000) Seafloor spreading around Australia. In: Veevers JJ (ed) Billion-year earth history of Australia and neighbours in Gondwanaland—BYEHA, pp 18–28

Murray J, Renard AF (1891) Deep-sea deposits based on the specimens collected during the voyage of H.M.S. Challenger in the years 1872 to 1876. Longmans, London, p 525

Nomura R (1991) Paleoceanography of Upper Maestrichtian to Eocene benthic foraminiferal assemblages at sites 752, 753 and 754, Eastern Indian Ocean. In: Weissel J, Peirce J, Taylor E et al (eds) Proc. ODP, Sci. Results, College Station, TX Ocean Drilling Program, pp 3–29

Olsson RK, Hemleben C et al (1999) Atlas of Paleocene planktonic Foraminifera. Smithsonian Institution, Washington, p 252

Pearson PN, Palmer MR (2000) Atmospheric carbon dioxide concentrations over the past 60 million years. Nature 406:659–699

Peterson MNA (1966) Calcite: rates of dissolution in a vertical profile in the central Pacific. Science 154:1542–1544

Proto-Decima F (1974) Leg 27 calcareous nannoplankton. In: Heirtzler JR, Veevers JJ, Bolli HM et al (eds) Init. Repts. DSDP, 27: Washington US Government Printing Office, pp 589–593

Quillevere F, Norris RD (2003) Ecological development of acariniids (planktonic Foraminifera) and hydrographic evolution of Paleocene surface waters. In: Wing SL, Gingerich PD, Schmitz B et al (eds) Causes and consequences of globally warm climates in the early Paleogene. The Geological Society of America, Spec. Paper 369, pp 223–238

Ravizza G, Norris RN et al (2001) An osmium isotope excursion associated with the late Paleocene thermal maximum; evidence of intensified chemical weathering. Paleoceanography 16:155–163

Rea DK, Lyle M (2005) Paleogene calcite compensation depth in the eastern subtropical Pacific: Answers and questions. Paleoceanography 20:PA1012. DOI 10.1029/2004PA001064

Robinson PT, Whitford DJ (1974) Basalts from the eastern Indian Ocean, DSDP Leg 27. In: Heirtzler JR, Veevers JJ, Bolli HM (eds) Init. Repts. DSDP, 27: Washington US Government Printing Office, pp 551–559

Shackleton NJ, Hall MA (1984) Carbon isotope data from Leg 74 sediments. In: Moore JTC, Rabinowitz PD, Boersma A et al (eds) Init. Repts. DSDP, 74: Washington US Government Printing Office, pp 613–619

Shipboard Scientific Party (1974) Site 259. In: Heirtzler JR, Veevers JJ, Bolli HM et al (eds) Init. Repts. DSDP, 27: Washington US Government Printing Office, pp 15–29

Shipboard Scientific Party (1990) Site 766. In: Gradstein FM, Ludden JN, Adamson AC et al (eds) Proc. ODP Init. Reps, 123: College Station, TX Ocean Drilling Program, pp 269–352

Shipboard Scientific Party (2004) Leg 208 summary. In: Zachos JC, Kroon D, Blum P (eds) Proc. ODP, Init. Repts., 198, College Station, TX Ocean Drilling Program, pp 1–112

Stott LD, Kennett JP (1990) Antarctic Paleogene planktonic foraminifer biostratigraphy; ODP Leg 113, Sites 689 and 690. In: Barker PF, Kennett JP et al (eds) Proc. ODP, Sci. Results, 113: College Station, TX Ocean Drilling Program, pp 549–565

Thomas E (1990) Late Cretaceous through Neogene deep-sea benthic foraminifers (Maud Rise, Weddell Sea, Antarctica). Proc ODP Sci Results 113:571–594

Thomas E (1998) The biogeography of the late Paleocene benthic foraminiferal extinction. In: Aubry MP, Lucas SG, Berggren WA (eds) Late Paleocene–early Eocene climatic and biotic events in the marine and terrestrial records, Columbia University Press, New York, pp 214–243

Thomas E, Shackleton NJ (1996) The Paleocene–Eocene benthic foraminiferal extinction and stable isotope anomalies. In: Knox RWOB, Corfield RM, Dunay RE (eds) Correlation of the early Paleogene in Northwest Europe, 101 Geological Society London Special Publication, pp 401–441

Thomas E, Zachos JC (1999) Deep-sea faunas during the late Paleocene–early Eocene climate optimum; boredom or boredom with short periods of terror? Geological Society of America, 1999 annual meeting, 31: Anonymous Geological Society of America (GSA), p 122

Thomas E, Zachos JC (2000) The late Paleocene thermal maximum a unique event? GFF 122:169–170

Thomas E, Zachos JC et al (2000) Deep-sea environments on a warm earth: latest Paleocene–early Eocene. In: Huber BT, MacLeod K, Wing SL (eds) Warm climates in Earth history. Cambridge University Press, Cambridge, pp 132–160

Thompson G, Bryan WB et al (1978) Basalts and related rocks from deep-sea drilling sites in the central and eastern Indian Ocean. Mar Geol 26:119–138

Thunell RC (1976) Calcium carbonate dissolution history in late Quaternary deep-sea sediments, western Gulf of Mexico. Q Res 6:281–297

Tjalsma RC, Lohmann GP (1983) Paleocene–Eocene bathyal and abyssal benthic foraminifera from the Atlantic Ocean. Micropaleontol Spec Publ 4:1–90

Toumarkine M, Luterbacher HP (1985) Paleocene and Eocene planktic foraminifera. In: Bolli HM, Saunders JB, Perch-Nielsen K (eds) Plankton stratigraphy, Cambridge University Press, Cambridge, pp 87–154

Tyrrell T, Zeebe RE (2003) History of carbonate ion concentration over the last 100 million years. Geochim Cosmochim Acta 68:3521–3530

Valyashko GM, Gorodnitskiy AM et al (1989) Tectonic evolution of Shatsky Uplift on the geomagnetic survey

van Andel TH (1975) Mesozoic/Cenozoic calcite compensation depth and the global distribution of calcareous sediments. Earth Planet Sci Lett 26:187–194

van Morkhoven FPCM, Berggren WA et al (1986) Cenozoic cosmopolitan deep-water benthic foraminifera. Bulletin des Centres de Recherches Exploration–Production Elf-Aquitaine, Memoire 11:421

Veevers JJ, Tayton JW (1985) Prominent magnetic anomaly along the continent-ocean boundary between the northwestern margin of Australia (Exmouth and Scott plateaus) and the Argo abyssal plain. Earth Planet Sci Lett 72:415–426

Widmark JGV (1997) Deep-sea benthic foraminifera from Cretaceous–Paleogene boundary strata in the South Atlantic-taxonomy and paleoecology. Fossils Strata 43:1–94

Williams DF, Gribble D et al (1985a) Dissolution and water-mass patterns in the Southeast Indian Ocean; Part II, The Pleistocene record from Brunhes to Matuyama age sediments. Geol Soc Am Bull 96:190–202

Williams DF, Healy-Williams N et al (1985b) Dissolution and water-mass patterns in the Southeast Indian Ocean; Part I, evidence from recent to late Holocene foraminiferal assemblages. Geol Soc Am Bull 96:176–189

Zachos J, Pagani M et al (2001) Trends, rhythms, and aberrations in global climate 65 Ma to present. Science 292:686–693

Zachos JC, Kroon D et al (2004) Proc. ODP, Init. Repts, 208 [Online]. Available from World Wide Web: http://www-odp.tamu.edu/publications/208_IR/208ir.htm. [Cited 2005–30-01]

Zachos JC, Rohl U et al (2005) Extreme acidification of the Atlantic Ocean at the Paleocene-Eocene Boundary (~ 55 Mya). Science 308:1611–1615. DOI 10.1126/science.1109004